

1 Supporting information for: Wilson *et al.* 2022. The role of spatial
2 structure in at-risk metapopulation recoveries.

3 In: *Ecological Applications*

4 **Appendix S1:** Overview of metapopulation model description & detailed results

5 Kyle L. Wilson^{1,2*}, Alexandra C. Sawyer¹, Anna Potapova¹, Colin J. Bailey¹, Daniella LoScerbo^{3,4},
Elissa K. Sweeney-Bergen^{1,5}, Emma E. Hodgson^{1,4}, Kara J. Pitman¹, Karl M. Seitz¹,
Lauren Law^{1,6}, Luke Warkentin^{1,7}, Samantha M. Wilson¹, William I. Atlas^{1,8},
Douglas C. Braun^{3,5}, Matthew R. Sloat⁸, M. Tim Tinker⁹,
and Jonathan W. Moore^{1,3}

¹Earth to Ocean Research Group, Simon Fraser University

²Central Coast Indigenous Resource Alliance, Campbell River, BC

³Resource and Environmental Management, Simon Fraser University

⁴Fisheries & Oceans Canada, Cultus Lake Laboratory, Cultus Lake, BC

⁵Ministry of Forests, Lands, Natural Resource Operations, and Rural Development, Smithers, BC

⁶Fisheries & Oceans Canada, Salmonid Enhancement Program, Nanaimo, BC

⁷Fisheries & Oceans Canada, North Coast Stock Assessment, Smithers, BC

⁸Wild Salmon Center, Portland, OR

⁹Ecology and Evolutionary Biology, University of California Santa Cruz

6 25 April 2023

7 **Contents**

8 Section S1.1: Metapopulation model	2
9 Section S1.1.1: Local & metapopulation dynamics	2
10 Section S1.1.2: Creating the spatial networks	3
11 Section S1.1.3: Dispersal	4
12 Section S1.1.4: Disturbance regimes	5
13 Section S1.1.5: Recruitment stochasticity	6
14 Section S1.2: Post-disturbance outcomes	7
15 Section S1.2.1: Monitoring & management at aggregate-scale	7
16 Section S1.2.2: Recovery metrics	7
17 Section S1.3: Scenarios	8
18 Section S1.3.1: Walkthrough of example results	10
19 Section S1.4: Sensitivity test of mean recovery metrics	16
20 Section S1.5: General patterns	17
21 Section S1.5.1: Effects of disturbance regime	17
22 Section S1.5.2: Role of interplay in ecological and disturbance conditions on recovery patterns	18
23 Section S1.6: Clustering analyses	23
24 Section S1.6.1: Emergent recovery outcomes	24
25 Section S1.6.2: Role of ecological and disturbance conditions on recovery outcomes	26
26 Section S1.7: References	28

*Corresponding author - email: klwilson.ccira@gmail.com

27 **Section S1.1: Metapopulation model**

28 **Section S1.1.1: Local & metapopulation dynamics**

29 Our metapopulation was defined by a set of P local populations for a species with a one year generation time with
 30 time-dynamics that follows birth (i.e., recruitment R), immigration, death, and emigration processes typical to
 31 metapopulation theory and tested the role of multiple local and regional processes (Anderson *et al.* 2015; Fullerton
 32 et al. 2016; Zelnik *et al.* 2019; Bowlby & Gibson 2020; Okamoto *et al.* 2020):

$$N_{i,t} = (1 - d_{i,t})(R_{i,t} + \sum_{\substack{j=1 \\ j \neq i}}^P \omega p_{i,j} R_{j,t} - \omega R_{i,t}) \quad (\text{S.1})$$

33 where $N_{i,t}$ was the number of adults in patch i at time t , $R_{i,t}$ was the number of recruits at time t , $\sum_{\substack{j=1 \\ j \neq i}}^P \omega p_{i,j} R_{j,t}$ was
 34 the number of recruits immigrating into patch i from any other patch, ω was the proportion of local recruits to
 35 disperse, $p_{i,j}$ was a distance-dependent dispersal function, and $d_{i,t}$ was the proportion of post-dispersal recruits lost
 36 from the disturbance regime.

37 Figure S1 shows how local patch recruitment at time t depended on adult densities at $t-1$ and followed a
 38 reparameterized Beverton-Holt function based on compensation ratio (see Box 3.1 in Walters & Martell 2004) and
 39 ignoring age-structure to model adult-to-adult dynamics, i.e., setting $\phi_{E_0} = 1$, $\phi_{B_0} = 1$ and $R_0 = N_0$ (see Table 3 in
 40 Forrest *et al.* 2010):

$$R_{i,t} = \frac{\alpha_i N_{i,t-1}}{1 + \frac{\alpha_i - 1}{\beta_i} N_{i,t-1}} \epsilon_{i,t} \quad (\text{S.2})$$

41 where α_i was the recruitment compensation ratio, β_i was local patch carrying capacity, and $\epsilon_{i,t}$ was lognormally
 42 distributed deviates to introduce stochastic recruitment dynamics.

43 Resource monitoring often occurs at the scale of the whole metapopulation by sampling aggregate abundances from
 44 multiple local populations to (Anderson *et al.* 2015; Moore *et al.* 2021), hence we define metapopulation adults as:

$$A_t = \sum_{i=1}^P N_{i,t} \quad (\text{S.3})$$

45 with metapopulation recruits:

$$K_t = \sum_{i=1}^P R_{i,t} \quad (\text{S.4})$$

46 Monitoring at the scale of the whole metapopulation can produce productivity relationships that aggregates the
 47 population dynamics and productivity among all local populations. For example, take a two patch metapopulation
 48 model (Figure S1) that each vary in demographic shape parameters $\alpha_1 = 2$; $\alpha_2 = 4$ and $\beta_1 = 100$; $\beta_2 = 200$. Here,
 49 recruitment compensation from local patches α_i gets averaged across the metapopulation leading to an average
 50 compensation ratio $\bar{\alpha}$ of 3. Likewise, the total carrying capacity of the metapopulation $\bar{\beta}$ becomes the summation
 51 of local patch carrying capacities $\sum \beta_i$, which was 300. This scale of monitoring generates the following local patch
 52 and metapopulation dynamics:

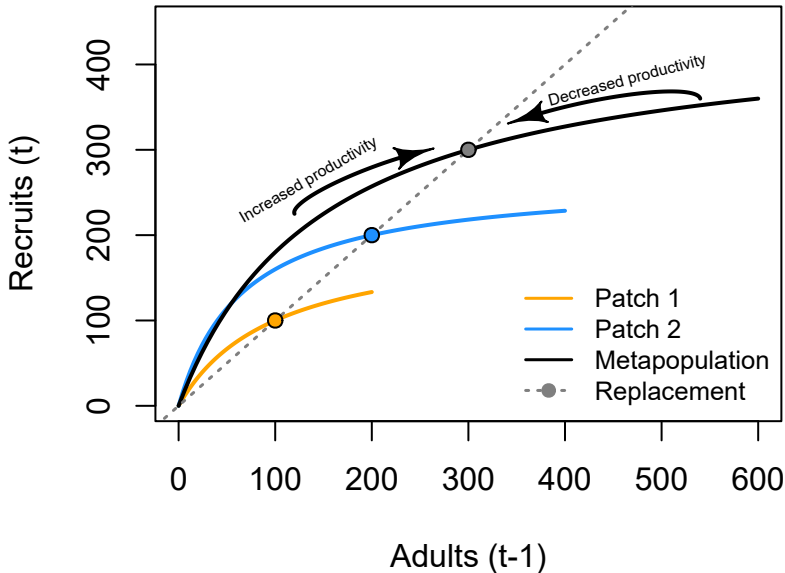


Figure S1: Density dependence in metapopulation and local patch recruitment dynamics. Dashed line indicates the line of replacement, with equilibrium indicated by points. When populations fall below equilibrium points, per-capita productivity improves driving populations back towards equilibrium. When populations exceed their capacity, per-capita productivity decreases driving populations back towards equilibrium. At each point of the x-axis, the distance between the solid and dashed lines indicates the amount of recruitment above replacement, i.e., the surplus recruitment produced via compensatory density dependence.

53 **Section S1.1.2: Creating the spatial networks**

54 The next aspect to developing our metapopulation model was connecting the set of patches to one another (Yeakel
 55 et al. 2014). We needed to specify the number of patches, their arrangements (i.e., connections), and how far apart
 56 they are from one another. We followed some classic metapopulation and source-sink arrangements to create four
 57 networks that generalize across a few real-world topologies: a linear habitat network (e.g., coastline), a dendritic or
 58 branching network (e.g., coastal rivers), a star network (e.g., mountain & valley, or lake with inlet tributaries), and
 59 a grid network (e.g., grasslands).

60 To make networks comparable, each spatial network type needs the same leading parameters (e.g., number of
 61 patches P and mean distance between neighboring patches \bar{d}). In this case, we set P to 16 and \bar{d} to 1 unit
 62 (distance units are arbitrary). We used the `igraph` package (Csardi & Nepusz 2006) to arrange our spatial
 63 networks as the following:

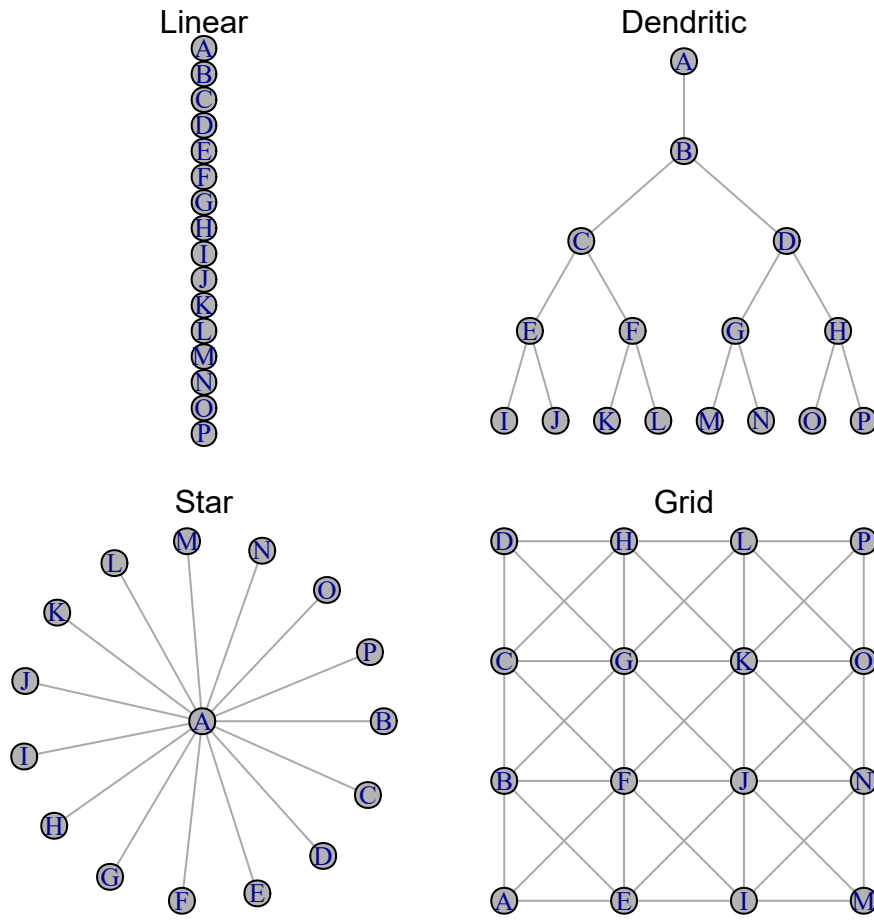


Figure S2: Four spatial network topologies.

Note that distances between neighbor patches in the above networks are equal. Table S1 shows an example dispersal matrix for a grid network.

Section S1.1.3: Dispersal

Dispersal from patch i into patch j depends on constant dispersal rate ω (defined as the proportion of total local recruits that will disperse) and an exponential distance-decay function between i and j with distance cost to dispersal m (Anderson et al. 2015; Fullerton et al. 2016):

$$E_{i,j,t} = \omega R_{i,t} p_{i,j} \quad (\text{S.5})$$

where $E_{i,j}$ was the total dispersing animals from patch i into patch j resulting from dispersal rate ω , total number of local recruits $R_{i,t}$, and probability of dispersal between patches $p_{i,j}$:

$$p_{i,j} = \frac{e^{-md_{i,j}}}{\sum_{\substack{j=1 \\ j \neq i}}^P e^{-md_{i,j}}} \quad (\text{S.6})$$

where $d_{i,j}$ was the pairwise distance between patches, m was the distance cost to dispersal. The summation term in the denominator normalizes the probability of moving to any patch to between 0 and 1 with the constraint that dispersers cannot move back into their home patch (i.e., $j \neq i$). With $\bar{d} = 1$, $m = 0.5$, $\omega = 0.1$, $R_{i,t} = 100$ in a linear

Table S1: Example distance matrix between 16 patches within a grid network to affect distance-dependent dispersal rates.

	A	B	E	F	C	G	D	H	I	J	K	L	M	N	O	P
A	0	1	1	1	2	2	3	3	2	2	2	3	3	3	3	3
B	1	0	1	1	1	1	2	2	2	2	2	2	3	3	3	3
E	1	1	0	1	2	2	3	3	1	1	2	3	2	2	2	3
F	1	1	1	0	1	1	2	2	1	1	1	2	2	2	2	2
C	2	1	2	1	0	1	1	1	2	2	2	2	3	3	3	3
G	2	1	2	1	1	0	1	1	2	1	1	1	2	2	2	2
D	3	2	3	2	1	1	0	1	3	2	2	2	3	3	3	3
H	3	2	3	2	1	1	1	0	3	2	1	1	3	2	2	2
I	2	2	1	1	2	2	3	3	0	1	2	3	1	1	2	3
J	2	2	1	1	2	1	2	2	1	0	1	2	1	1	1	2
K	2	2	2	1	2	1	2	1	2	1	0	1	2	1	1	1
L	3	2	3	2	2	1	2	1	3	2	1	0	3	2	1	1
M	3	3	2	2	3	2	3	3	1	1	2	3	0	1	2	3
N	3	3	2	2	3	2	3	2	1	1	1	2	1	0	1	2
O	3	3	2	2	3	2	3	2	2	1	1	1	2	1	0	1
P	3	3	3	2	3	2	3	2	3	2	1	1	3	2	1	0

75 network):

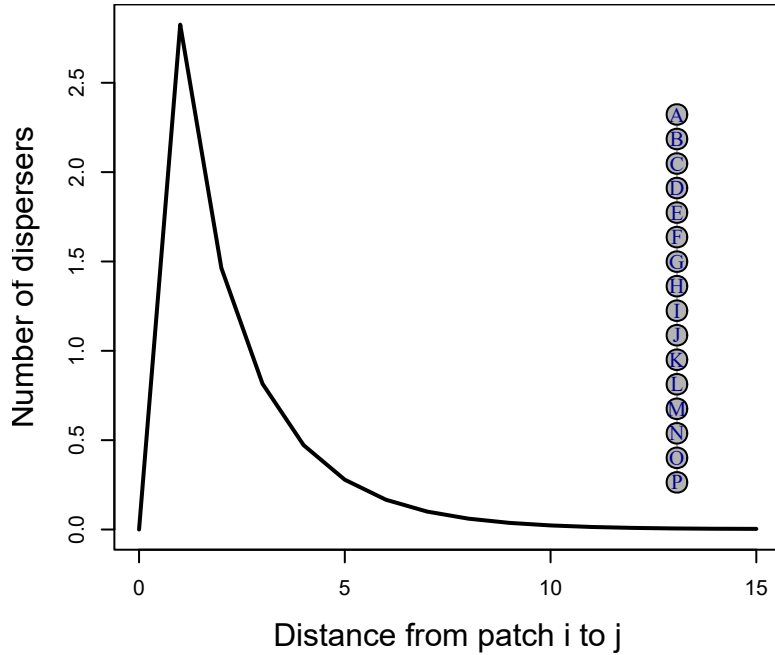


Figure S3: Example dispersal patterns across linear network.

76 **Section S1.1.4: Disturbance regimes**

77 In all scenarios, disturbance was applied after 50 years of equilibrating the metapopulation at pristine conditions.
 78 We then applied a pulsed disturbance regime at year 50 (the regime varied from *uniform*, *localized*, *even*, and
 79 *localized, uneven* - see *Scenarios* below). Disturbance immediately removed a fixed proportion of the
 80 metapopulation adults at that time (i.e., 0.9 of $A_{t=50}$). Once applied, the metapopulation was no longer disturbed
 81 and spatio-temporal recovery dynamics emerged from these conditions given the ecological scenarios of network
 82 complexity, dispersal rate, spatio-temporal correlations, local patch demographies, and magnitude of stochastic
 83 variance.

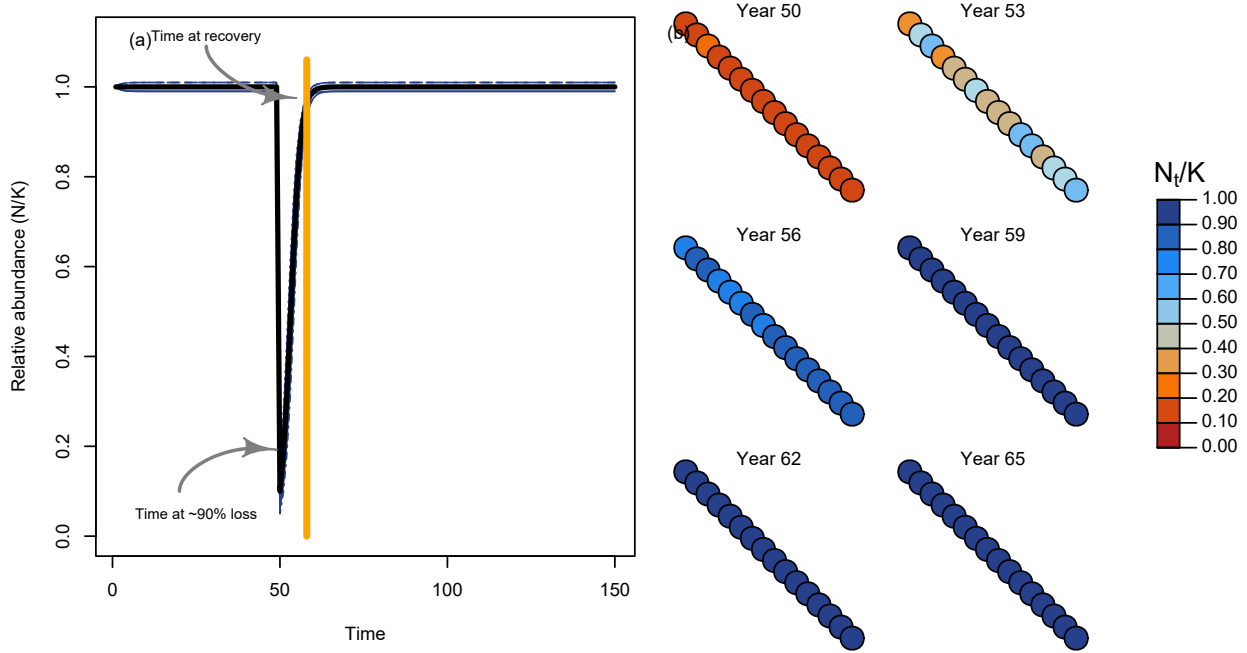


Figure S4: Recovery regime of metapopulation with linear topology through time (a) and space (b).

84 Section S1.1.5: Recruitment stochasticity

85 Our model allowed for stochastic recruitment that followed a lognormal distribution with average variation in
86 recruitment of σ_R . In cases with stochastic recruitment, the deterministic recruitment in eq. S.4 becomes:

$$R_{i,t} = \frac{\alpha_i N_{i,t-1}}{1 + \frac{\alpha_i - 1}{\beta_i} N_{i,t-1}} e^{(\epsilon_{i,t} - \frac{\sigma_R^2}{2})} \quad (\text{S.7})$$

87 where lognormal deviates for each patch i at time t were drawn from a multivariate normal distribution (MVN)
88 with bias correction $\frac{\sigma_R^2}{2}$. If σ_R was low, then metapopulation dynamics approach the deterministic case. In some
89 scenarios, we evaluated the role of spatially and/or temporally correlated deviates among local patches to model
90 potential common drivers affecting metapopulation dynamics (e.g., Moran effects). Expected recruitment deviates
91 followed a first-order autoregression model such that:

$$\epsilon_{i,t} = \rho_T \epsilon_{t-1} + MVN(\mu = 0, \Sigma = \sigma_R^2(1 - \rho_T^2)e^{-\rho_S D_{i,j}}) \quad (\text{S.8})$$

where ρ_T was temporal correlation (bounded $0 - 1$) and ρ_S was rate of distance-decay in spatial correlation (bounded $0 - \infty$ with higher values leading to independent patches). If ρ_T was 0 and ρ_S was high, then annual recruitment deviates were independent. We modelled the initial conditions for autoregressive recruitment deviates $\epsilon_{i,1}$ by drawing from a stationary normal distribution with mean $\mu = 0$ and variance σ_R^2 such that:

$$\epsilon_{i,1} \sim N(\mu = 0, \sigma = \sigma_R) \quad (\text{S.9})$$

92 We illustrate the effects of four kinds of recruitment deviates below using the same random number generator seed:

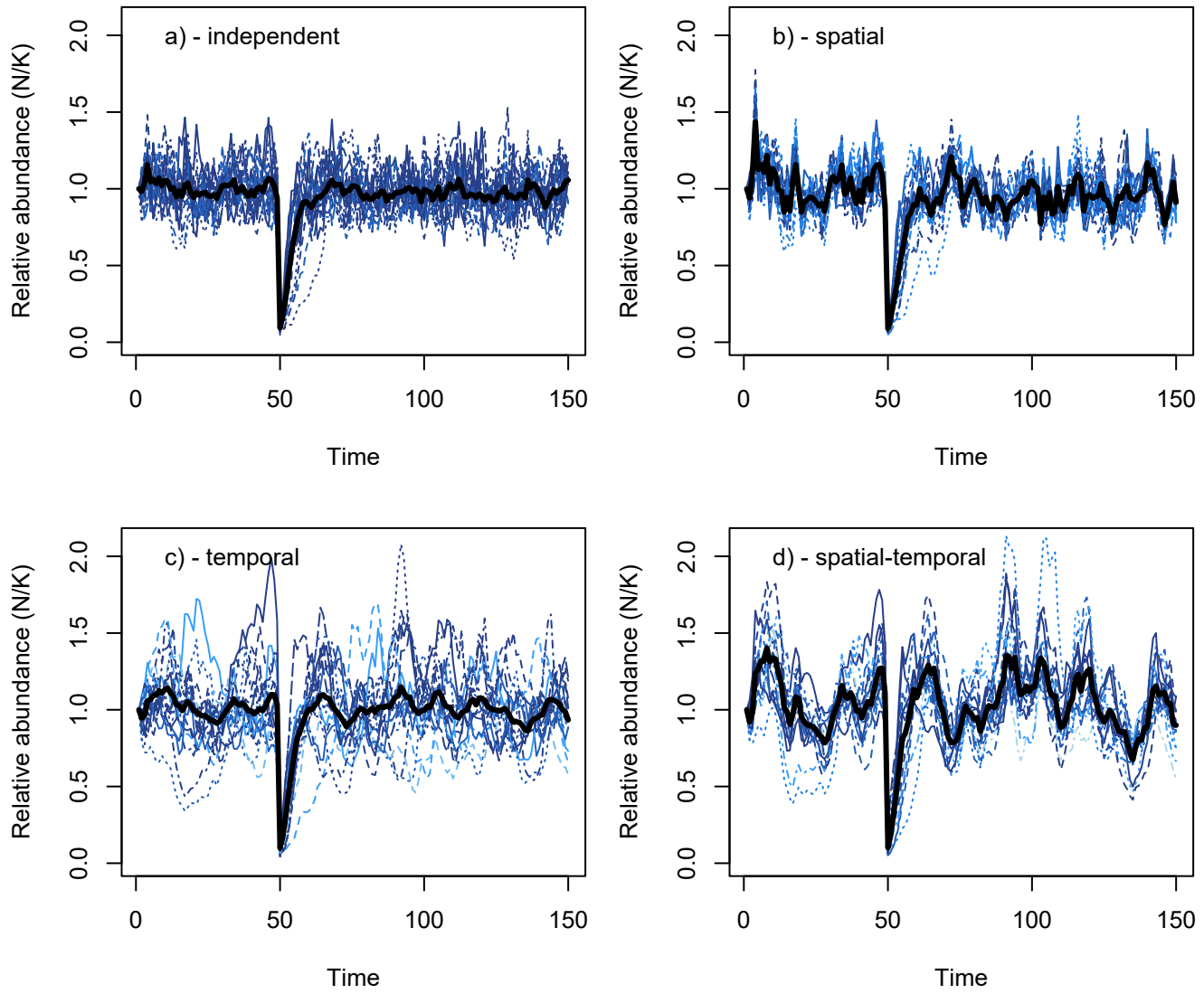


Figure S5: Metapopulation dynamics with independent (a), spatially correlated (b), temporally correlated (c), and spatio-temporally correlated (d) recruitment deviates. Black line indicates metapopulation, and dashed lines indicate local patches with red and blue relating to abundances after 100 years post-disturbance were less than or greater than 1.0 pre-disturbance, respectively.

93 Section S1.2: Post-disturbance outcomes

94 Section S1.2.1: Monitoring & management at aggregate-scale

95 While true metapopulation dynamics emerge from local patch dynamics and dispersal in eq. S.1, natural resource
 96 managers often monitor and manage at the scale of the metapopulation. Hence, management at this scale
 97 inherently defines the stock-recruitment dynamics of the aggregate complex of patches (i.e., metapopulation) as:

$$\mathbb{E}(N_t) = \frac{\bar{\alpha}A_{t-1}}{1 + \frac{\bar{\alpha}-1}{\bar{\beta}}A_{t-1}} \quad (S.10)$$

98 where $\bar{\alpha}$ was the compensation ratio averaged across the metapopulation and $\bar{\beta}$ was the carrying capacity summed
 99 across the entire metapopulation.

100 Section S1.2.2: Recovery metrics

101 We measured the following post-disturbance outcomes to track the temporal and spatial recovery regime of the
 102 metapopulation.

- 103 1. Recovery rate after disturbance: Recovery rate represents the inverse proportion of the post-disturbance
 104 phase that the metapopulation took to recover. Recovery rate was calculated as $1 - T_{recovery}/T_{sim}$ where the
 105 recovery time, $T_{recovery}$, was the number of years/generations (1 year = 1 generation in our models) it took
 106 for the metapopulation to reach five consecutive years pre-disturbance abundance. Recovery rate captures
 107 how quickly the aggregate metapopulation recovers from disturbance but doesn't take into account whether
 108 any given local patches recover to their pre-disturbance capacity nor did it allow for any uncertainty around
 109 recovery criteria.
- 110 2. Patch occupancy: The number of patches with >0.1 local carrying capacity after disturbance in the
 111 short-term (5 years), medium-term (10 years), and long-term (25 years). This value characterizes the
 112 expected risk of spatial contractions or local patch collapses, and reflects how interactions between spatial
 113 structure, disturbance, and dispersal shape source-sink dynamics and the ability to provide (or not) rescue
 114 effects and recover local patches.
- 115 3. Relative production: The ratio between the empirical metapopulation adult abundances to the expected adult
 116 recruitment if the metapopulation were a single, contiguous population of equivalent size and productivity
 117 (i.e., carrying capacities and productivity were equal to the sum β and mean α among patches, respectively).
 118 We term Δ_N by calculating the stock-recruitment model to aggregate metapopulation adults (eq. S.10) such
 119 that:

$$\Delta_{N_t} = \frac{A_t}{\mathbb{E}(N_t)} \quad (\text{S.11})$$

120 A value of 1.0 would indicate that the disturbed metapopulation production was equal to a single, contiguous
 121 population such that source-sink dynamics were not consuming surplus recruits. In other words, this metric
 122 can describe whether the metapopulation acts more than ($\Delta_{N_t} > 1.0$), less than ($\Delta_{N_t} < 1.0$), or equal to the
 123 sum of its parts ($\Delta_{N_t} = 1.0$).

- 124 4. Risk of non-recovery after disturbance: Non-recovery rate was defined as the % of simulations where
 125 metapopulation abundance failed to recover to 1.0 of the average pre-disturbance abundance for 5
 126 consecutive years post-disturbance. This "non-recovery rate" reflects the risk of a long-term state shift in
 127 metapopulation dynamics after disturbance in the face of stochasticity.

128 Section S1.3: Scenarios

129 We tested all combinations of the following eight processes (below) and ran 100 stochastic iterations per scenario
 130 (see section on *Sensitivity test of mean recovery metrics* below) to estimate the mean outcome for each of the above
 131 recovery metrics:

- 132 1. Homogenous and spatially variable recruitment compensation ratio across patches, i.e. intrinsic rate of
 133 population growth (α_i).
- 134 a. when **variable**, $\alpha_i \sim TN(\mu = \bar{\alpha}, \sigma_\alpha = 0.3\bar{\alpha})$ with a truncation applied such that $5 \leq \alpha_i \geq 1$ to ensure
 135 that patches could, at minimum, could replace themselves but with an upper limit of a 5-fold
 136 improvement to per-capita productivity. By comparison, Myers et al. (1999) found that compensation
 137 ratio (their $\hat{\alpha}$) ranged 1-7 for most species evaluated. Since our focus was on at-risk species, we opted to
 138 truncate α_i towards the lower end of this range, with a mean of 2.0.
- 139 2. Homogenous and spatially variable local carrying capacity across patches, i.e. asymptote of expected recruits
 140 at high adult densities (β_i)
- 141 a. when **variable**, $\beta_i \sim \text{multinomial}(p_i, N)$ where $p_i = \frac{e^{\theta_i}}{\sum e^{\theta_i}}$, $\theta_i \sim \text{uniform}(0, 1)$, and $N = \bar{\beta}$, with the
 142 added constraint that $\beta_i < 0.1\bar{\beta}$ to ensure that no one patch exceed 10% of total metapopulation
 143 abundance (a necessary constraint when modelling *local, even* and *local, uneven* disturbances below).
 144 Note that, when local variation in demography rates occurred, the truncated normal in *Appendix S1: Section S1.3.1.a* and truncated multinomial in *Appendix S1: Section S1.3.2.a* above led compensation
 145 ratio and carrying capacity, respectively, to vary by the same magnitude ~28% coefficient of variation
 146 (Appendix S1: Figure S6).
- 148 3. Variation in the spatial distribution of disturbances where a proportion of individuals were removed from the
 149 metapopulation (e.g., 0.90) occurs.
- 150 a. *uniform* - individuals randomly removed across all patches, with all individuals having equal

- vulnerability to being removed.
- b. *local, even* - randomly chosen individuals removed from random subset of patches (as long as the target individuals lost in the metapopulation can be achieved in that subset of patches)
- i. Specifically, a numerical algorithm was used to search and find a set of disturbance conditions whereby removing a random proportion of individuals from a random subset of local patches achieved both:
 - a total loss that summed to a ~90% loss in abundance to the whole metapopulation, and
 - left at least one local patch *undisturbed* to start metapopulation recoveries.
- c. *local, uneven* - total extirpation of randomly selected subset of patches (as long as the target individuals lost in the metapopulation can be achieved in that subset of patches).
- i. Specifically, a numerical algorithm was used to search and find a set of disturbance conditions whereby extirpations to a random subset of local patches achieved both:
 - a total loss that summed to a ~90% loss in abundance to the whole metapopulation, and
 - left at least one local patch *undisturbed* to start metapopulation recoveries.
4. Density-independent dispersal rates ω from 0 to 5% of individuals within a patch will disperse.
5. Topology of the spatial networks with linear, dendritic, star, and grid networks. Each network with $P = 16$ and distance between patches $\bar{d} = 1$.
6. Stochastic recruitment deviates with low, medium, and high standard deviation in lognormal error. Used to generate stochastic population dynamics via random deviates from the expected recruitment relationship in eq. S.2.
7. Temporal correlation in recruitment deviates from low, medium, and high correlation (i.e., good year at time t begets good year at time $t+1$).
8. Spatial correlation in recruitment deviates among patches from low, medium, to high correlation (i.e., neighboring patches go up or down together).

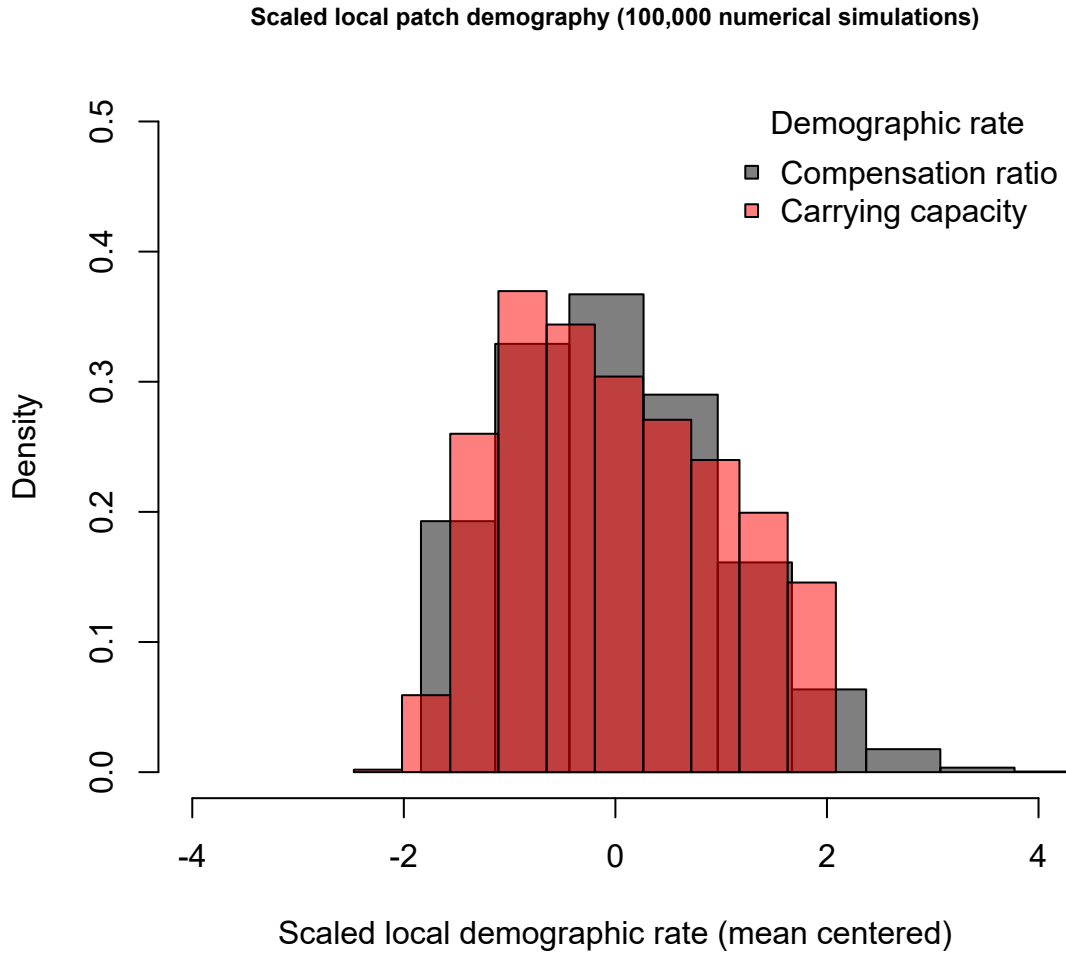


Figure S6: Histogram showing variation among demographic rates after simulating 100,000 local patches when using the truncated normal in Appendix S1: Section 1.3(1.a) and truncated multinomial in Appendix S1: Section 1.3(2.a) when modelling variation in local compensation ratio (grey) and carrying capacity (red).

¹⁷⁵ **Section S1.3.1: Walkthrough of example results**

¹⁷⁶ We demonstrate our metapopulation model with an example outcome for a linear network composed of 16 patches,
¹⁷⁷ a dispersal rate of 0.01 and a high enough dispersal cost such that individuals are only willing to move to their
¹⁷⁸ closest neighboring patches. This limits the strength of potential rescue effects. For this example, patches varied in
¹⁷⁹ their productivity and carrying capacity but will have deterministic population dynamics.

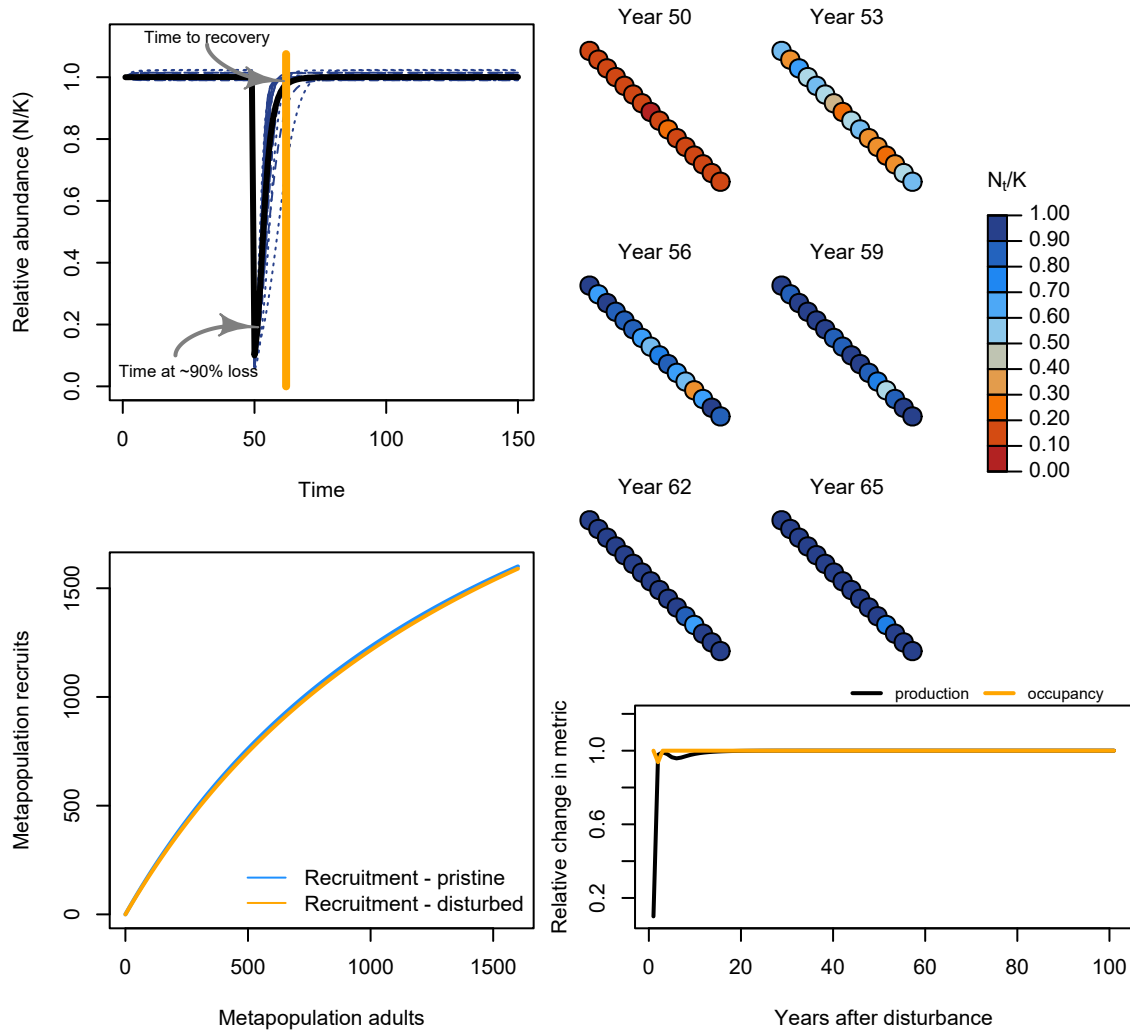


Figure S7: Example iteration of spatial recovery regime of metapopulation with linear topology through time (top left) and space (top right). Recruitment dynamics before and 10 years after disturbance (bottom left). Relative bias in aggregate-scale estimates of carrying capacity, compensation ratio, and recruitment production in recovery phase (bottom right).

¹⁸⁰ We can then contrast this with a different network shape, like a dendritic network.

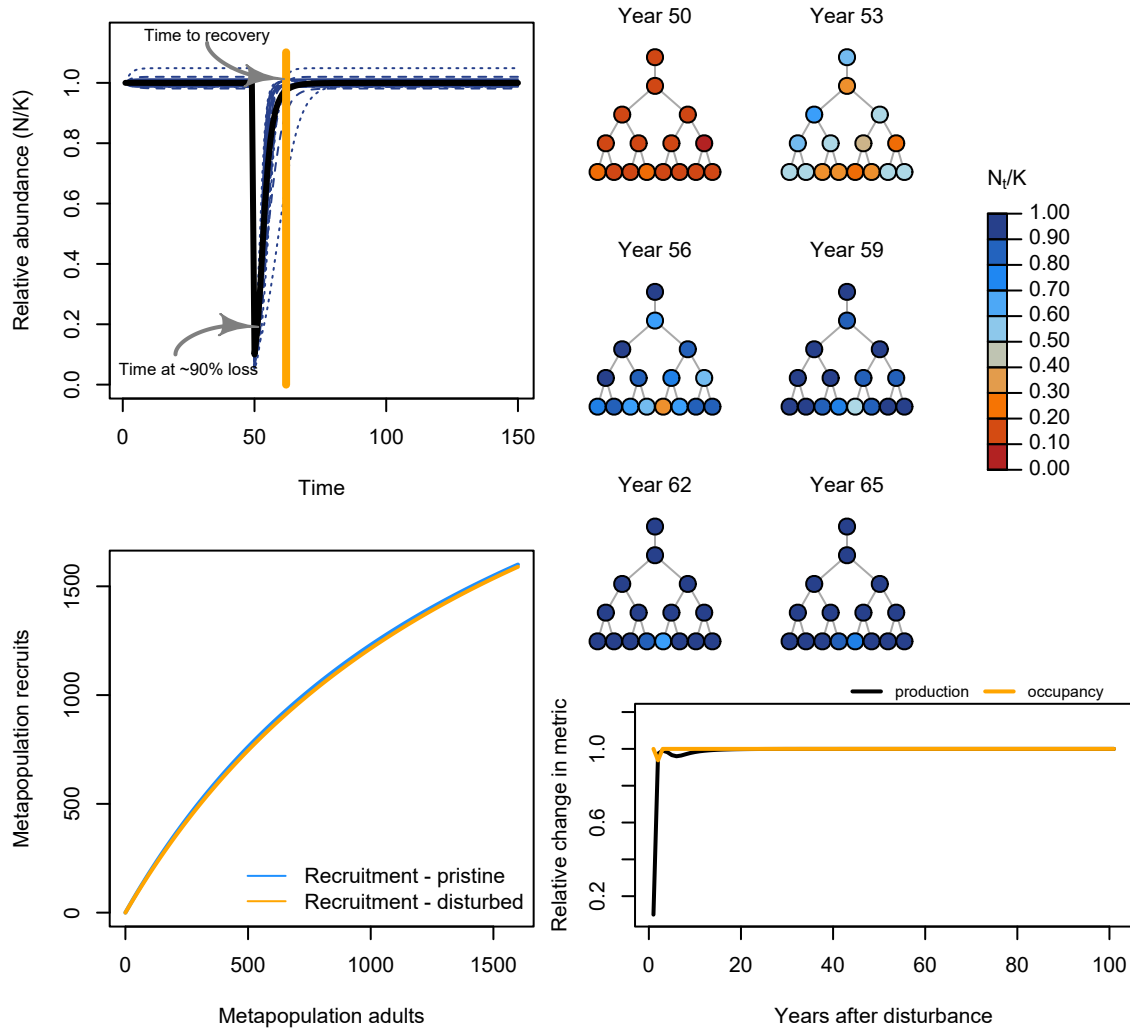


Figure S8: Example iteration of spatial recovery regime of metapopulation with dendritic topology.

¹⁸¹ Now, let's add some stochasticity to recruitment and see how this affects the recovery regime.

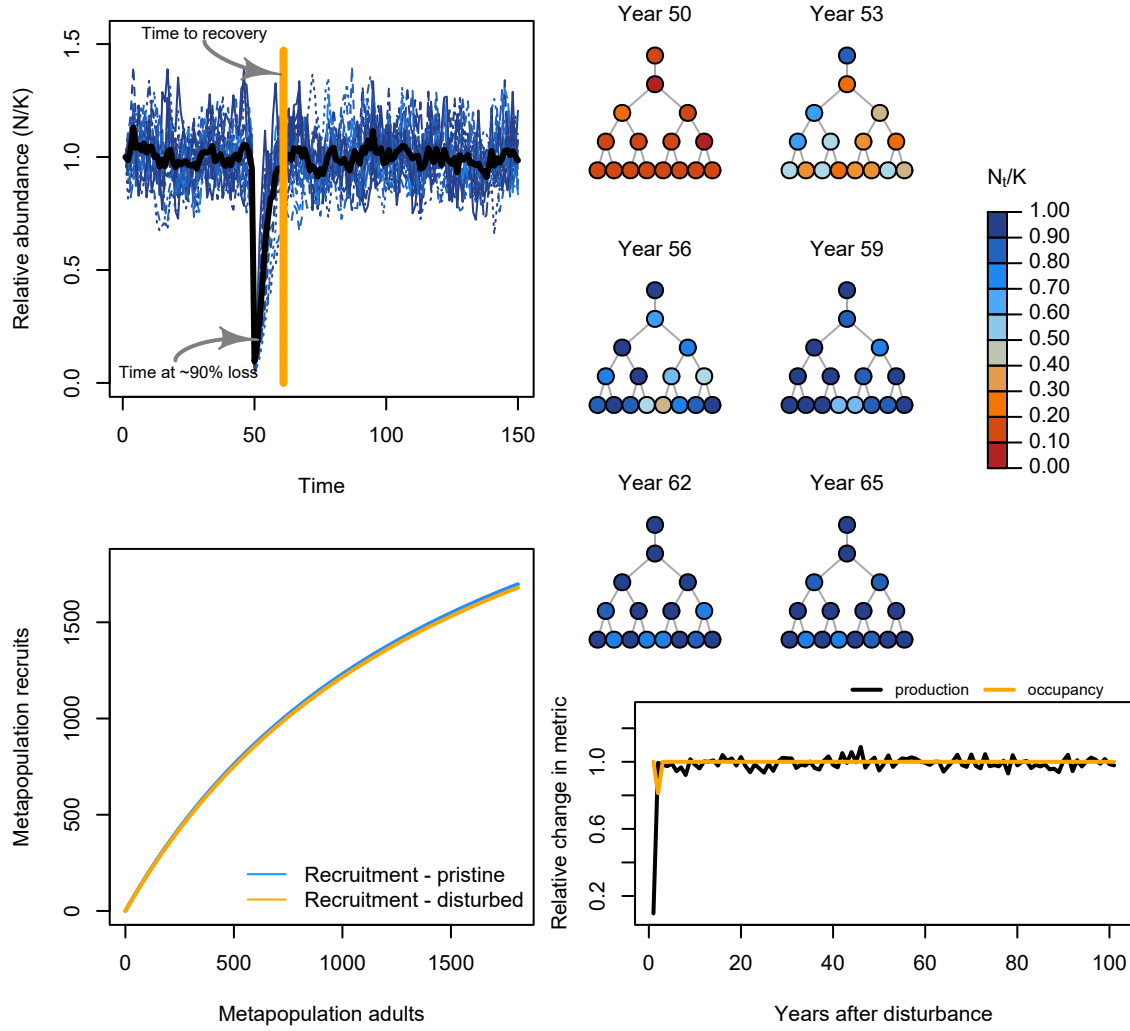


Figure S9: Example iteration of spatial recovery regime of stochastic metapopulation.

¹⁸² Next, we can contrast with a disturbance regime where the disturbance is locally even among a subset of local
¹⁸³ patches (rather than uniform across all patches or local extirpations).

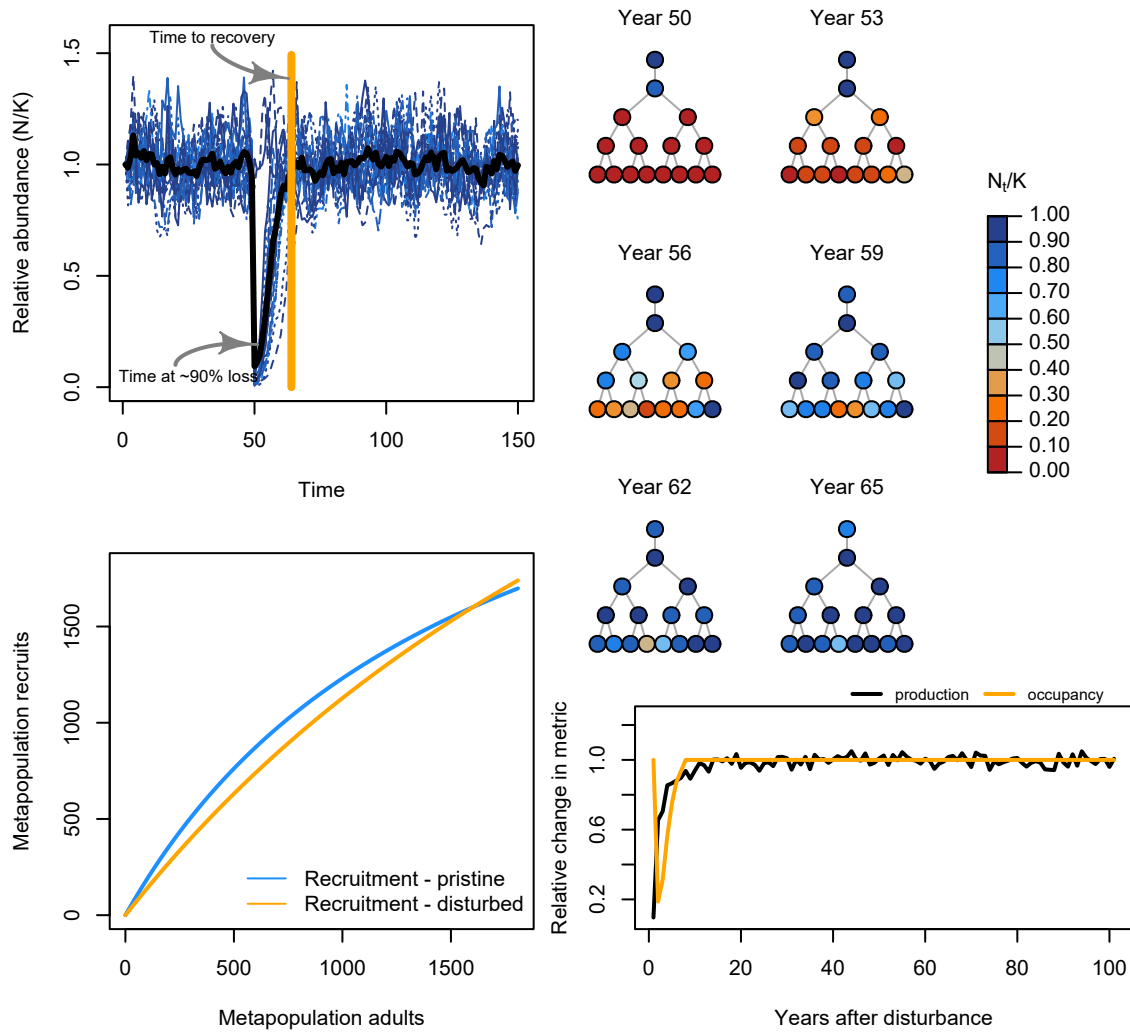


Figure S10: Example iteration of spatial recovery regime of stochastic metapopulation.

184 Next, we can contrast with a disturbance regime where the disturbance is concentrated on local patches that can
 185 be completely extirpated (rather than the disturbance being applied proportionally across all patches e.g., a
 186 mixed-stock fishery).

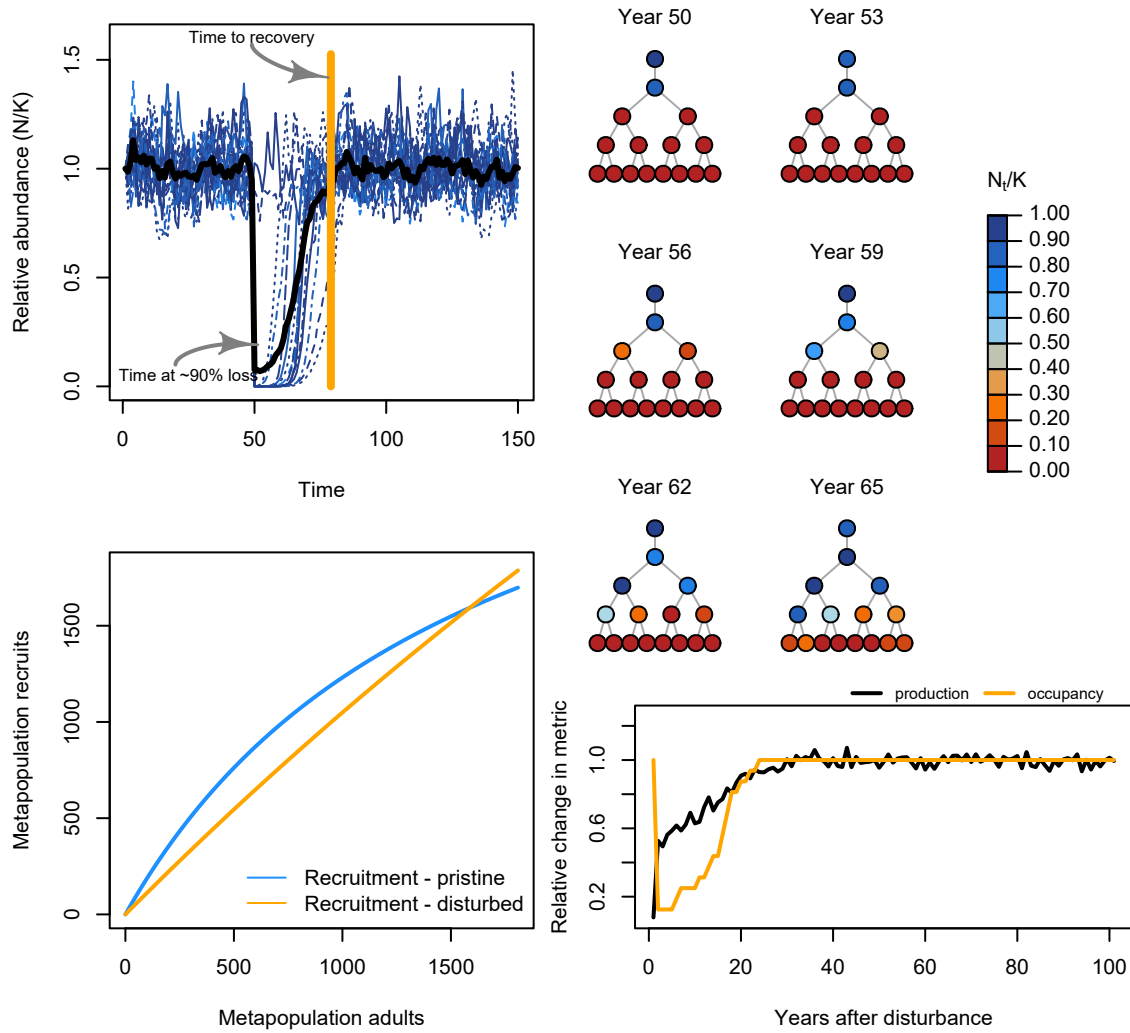


Figure S11: Example iteration of spatial recovery regime of stochastic metapopulation.

¹⁸⁷ **Section S1.4: Sensitivity test of mean recovery metrics**

¹⁸⁸ The total number of scenarios resulted in a long computation time to run all simulations a large number of times
¹⁸⁹ necessary to evaluate how metapopulation responded, on average, to our ecological and disturbance scenarios. To
¹⁹⁰ determine a sufficient number of bootstrap iterations to run, we ran a sensitivity test to explore the relative
¹⁹¹ sensitivity of the mean for a few recovery metrics of interest (recovery rate) to the number of stochastic simulations
¹⁹² ran per scenario. Below, we repeated the scenario for a metapopulation with a dendritic network, with high
¹⁹³ stochasticity, locally uneven disturbances, large spatial-temporal correlations, variable patch productivities, and
¹⁹⁴ variable patch capacities along gradients of 10, 100, 500, and 1,000 stochastic simulations. Based on these
¹⁹⁵ preliminary results, we see that the mean for most metrics was relatively insensitive with at least 100 simulations.

Average recovery metrics

Sensitivity of mean recovery metrics to the number of stochastic simulations

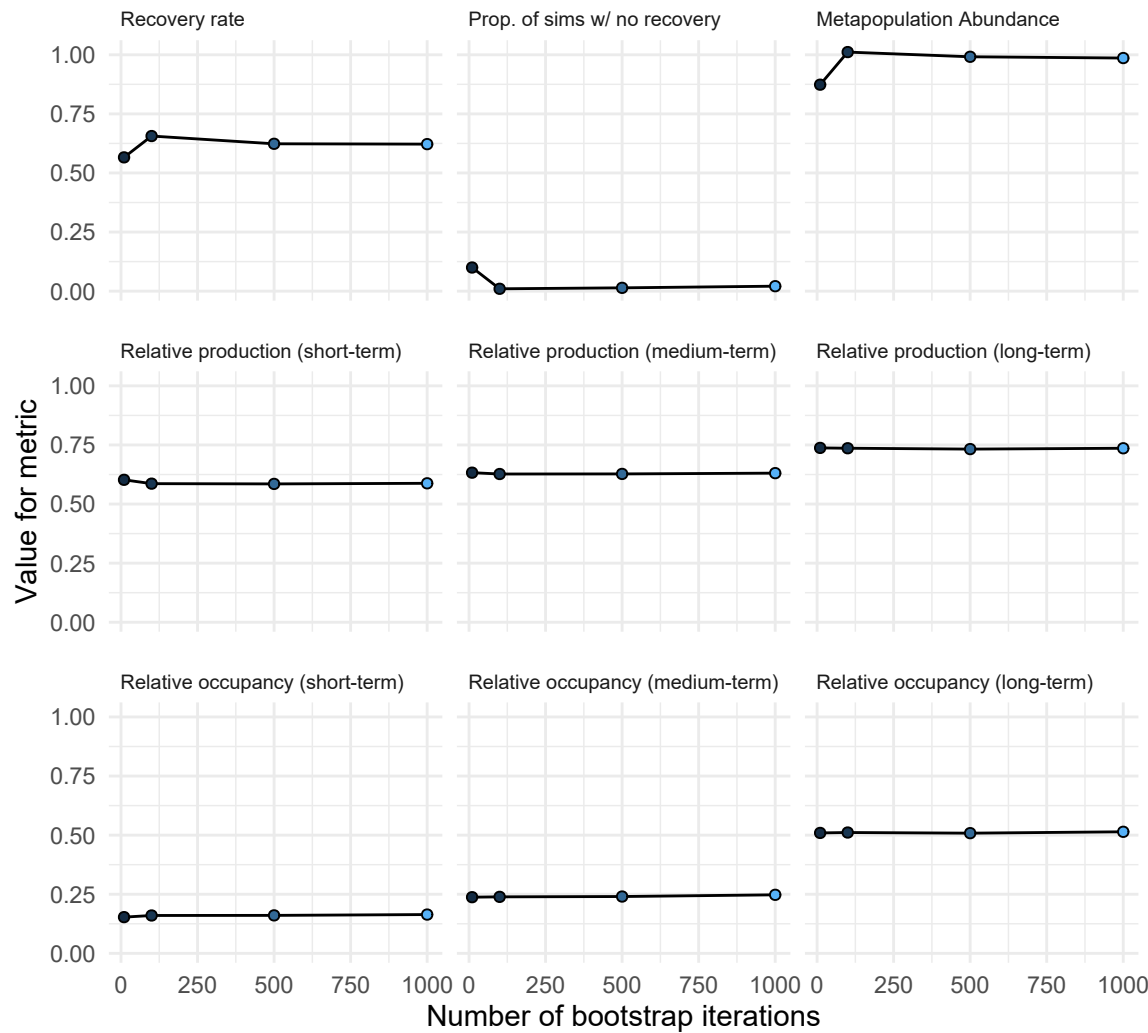


Figure S12: Sensitivity test of mean recovery metrics to number of iterations to bootstrap the stochastic simulations. Example metapopulation consisted of a dendritic network, high recruitment stochasticity, locally uneven disturbance regime, large spatial-temporal correlations, variable patch productivities, and variable patch capacities tested along gradients of 10, 100, 500, and 1,000 bootstrapped iterations.

196 **Section S1.5: General patterns**

197 **Section S1.5.1: Effects of disturbance regime**

198 The strongest lever influencing recovery in our simulated metapopulations was, by far, the characteristics of the
 199 disturbance regime. Specifically, the degree to how locally concentrated the disturbance was on the set of patches
 200 was more influential than variation in local demographic rates, dispersal rates, or network topology. Localized
 201 disturbances increased the risk of spatial contraction, reduced recovery rates and aggregate compensation, and
 202 increased the risk of non-recoveries. By altering aggregate compensation, localized disturbance reduced the relative
 203 production of the metapopulation. In other words, through changes in source-sink dynamics, metapopulations
 204 under localized disturbance acted less than the sum of their parts – the more localized the impacts, the worse these
 205 effects. Uniform disturbances generally left the metapopulation dynamics unaffected with few changes to recovery
 206 metrics outside of occasionally slower recoveries. These above spatial and temporal recovery processes also
 207 appeared tied to one another such that changes to any of them had feedbacks with other recovery metrics. Perhaps
 208 intuitively, for example, patch occupancy was highly correlated to the relative production of the metapopulation,
 209 such that the more patches occupied, the more that metapopulation dynamics resembled a contiguous population.

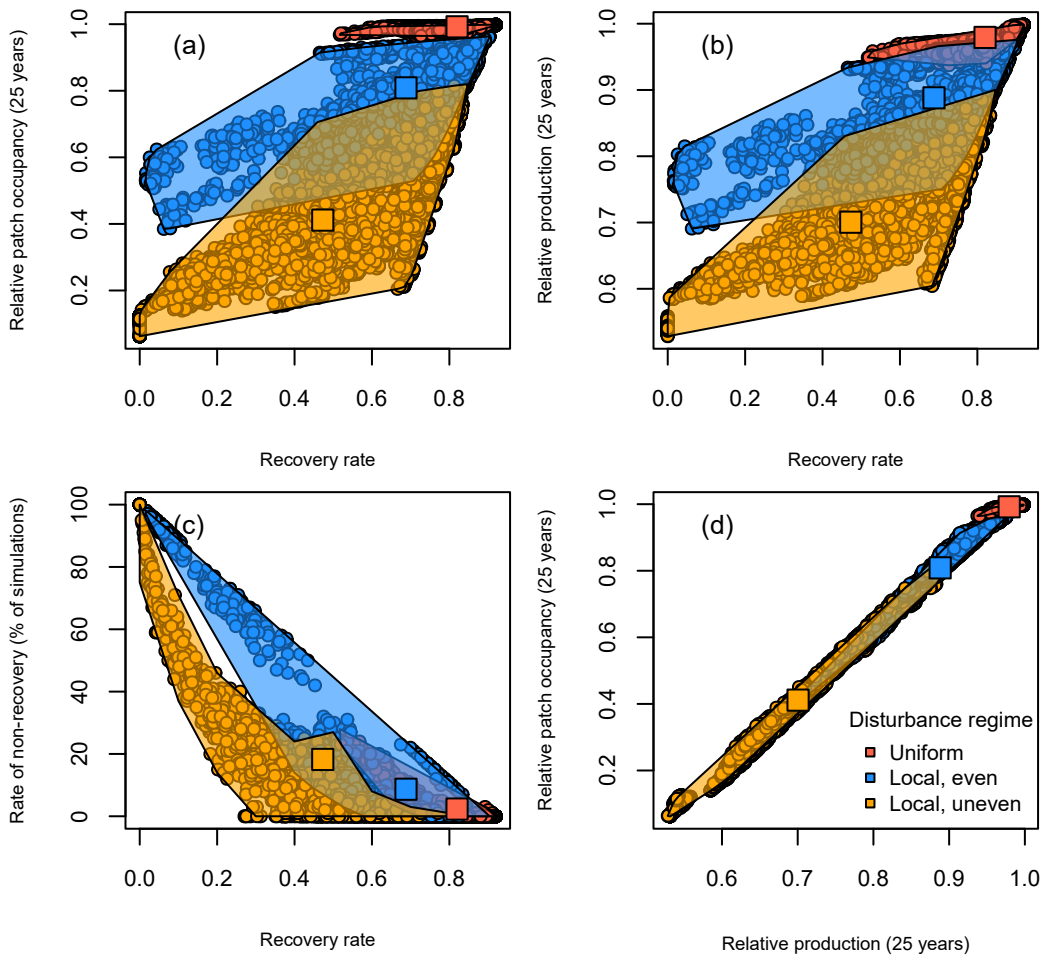


Figure S13: The role of spatial disturbance regimes on metapopulation recoveries and covariation among four recovery metrics: (a,b,c) recovery rate – the annual rate of metapopulation recovery; (a,d) relative patch occupancy – the mean proportion of patches occupied 25 years after disturbance; (b,d), relative production – the ratio between the summed abundances across all patches to the expected production of an equivalent single population 25 years after disturbance; and (c) rate of non-recovery – the percent of 100 stochastic simulations where the metapopulation failed to recover. Each point represents a single simulation for a metapopulation under a unique combination of local productivity, dispersal, spatial network, stochasticity, and disturbance (9,504 total simulations). Shaded regions describe the range in recovery metrics for all simulated metapopulations and are colored by disturbance regime. Square points represent the mean recovery metrics from all simulations within each disturbance regime.

210 **Section S1.5.2: Role of interplay in ecological and disturbance conditions on recovery patterns**

211 We now show some general patterns in how variable patch demographic rates, network structure, dispersal,
 212 disturbance, recruitment stochasticity, and spatio-temporal correlations variation affects metapopulation *recovery*
 213 *rates* (shown in Figure 4 of the main text and Figure S13 & S15), *non-recovery rate* (i.e., the number of simulations
 214 where the metapopulation fails to recover; Figure S16), *patch occupancy* (i.e., number of patches with local
 215 abundance <10% of pre-disturbance; Figure S17), and *relative production* (Figure S18).

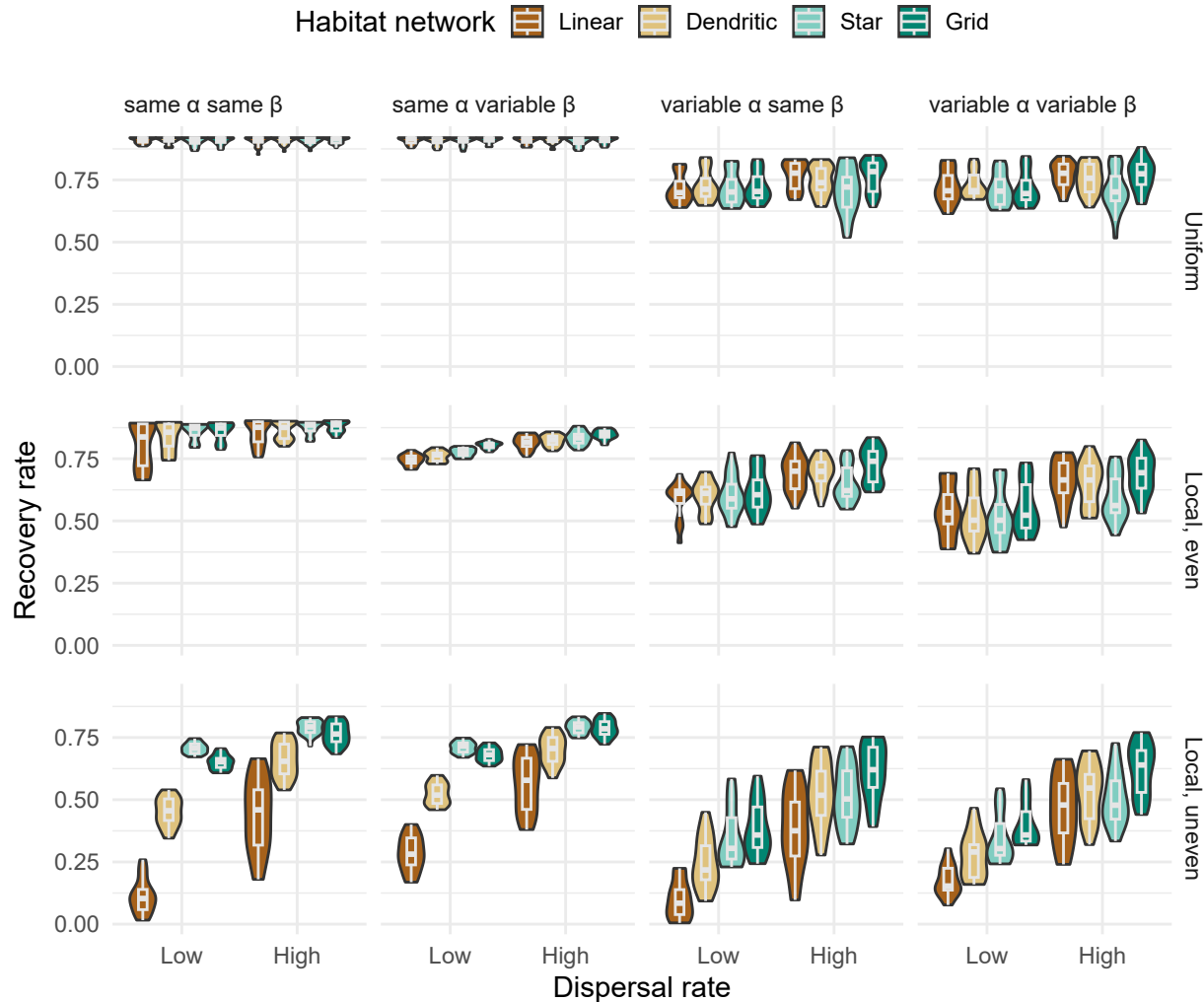


Figure S14: Violin plots showing marginal response of metapopulation recovery rates along gradients of network configuration, dispersal categories (low 0.001; high >0.001), heterogeneity in local demographic rates (α was local patch productivity and β was local patch carrying capacity in the Beverton-Holt model), and spatial distribution of disturbance.

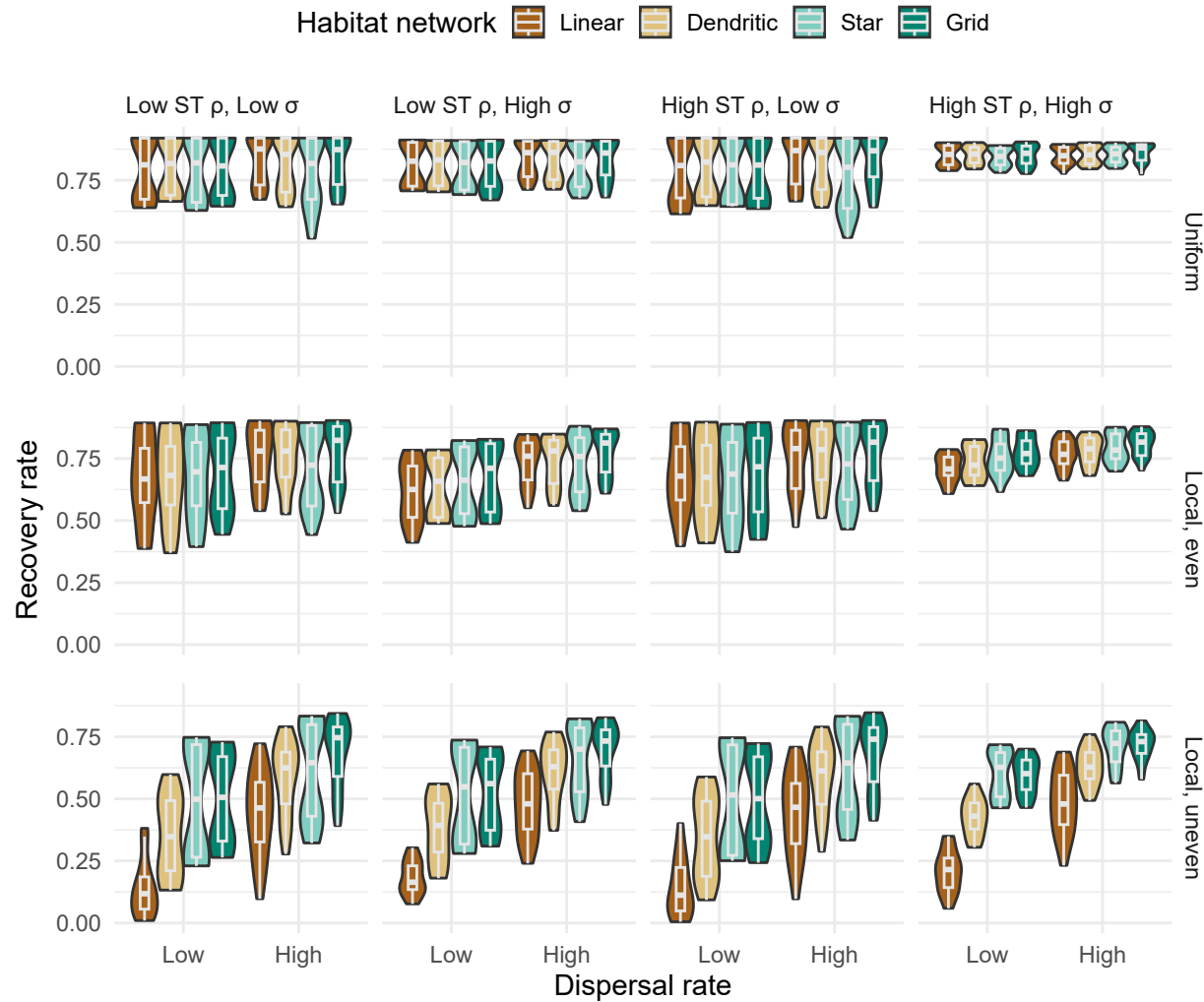


Figure S15: Violin plots showing marginal response of metapopulation recovery rates along gradients of network configuration, dispersal categories (low 0.001 ; high >0.001), spatial-temporal (ST) correlations (low $\rho=0$; high $\rho=0.6$), scale of lognormal variance in recruitment (low $\sigma=0.001$; high $\sigma=0.1$), and spatial distribution of disturbance.

²¹⁶ Next, we show violin plots demonstrating some of the modulating factors leading to variation in the risk of
²¹⁷ non-recovery owing to stochastic recruitment dynamics.

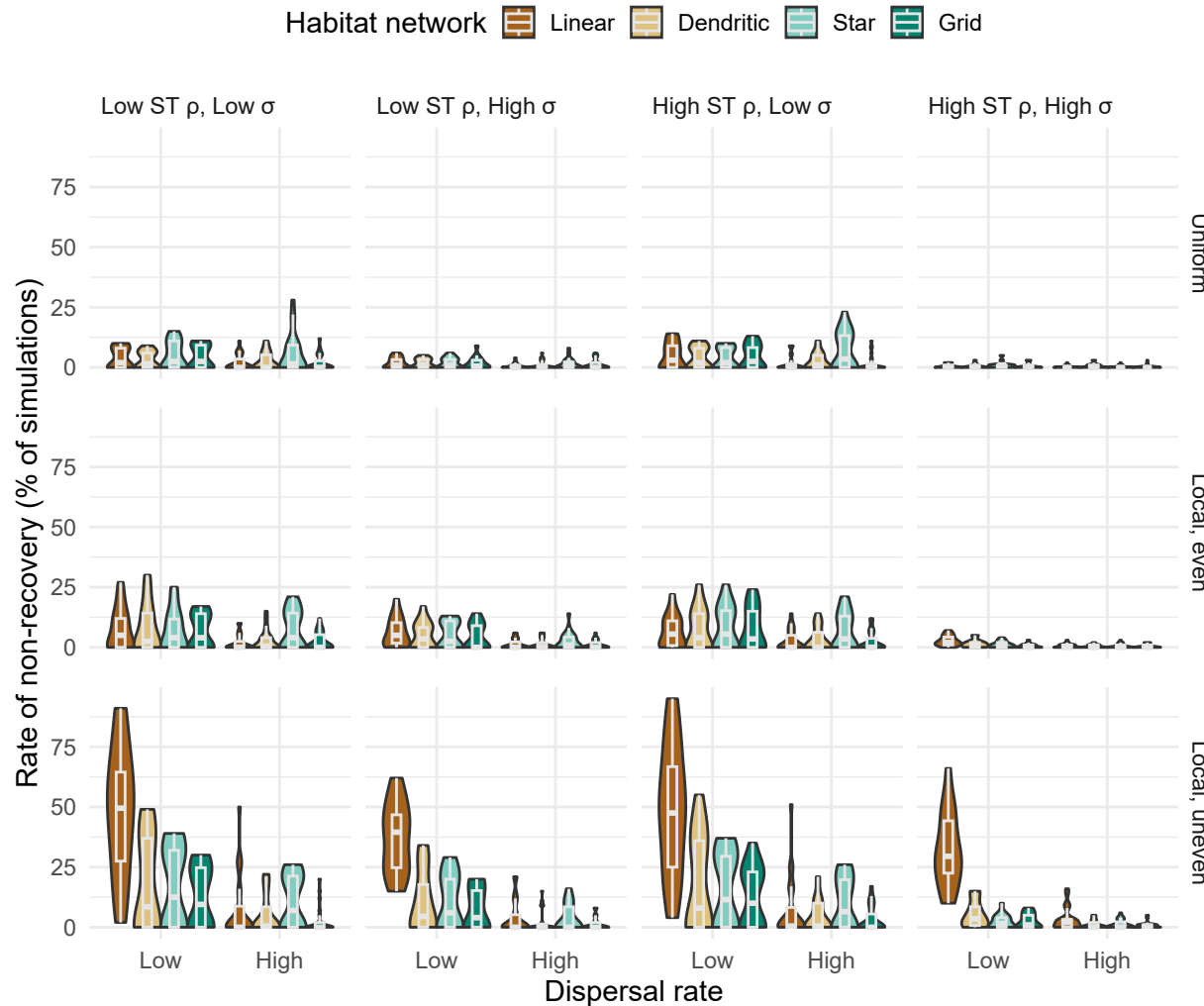


Figure S16: Violin plots showing marginal response of the stochastic risk of non-recovery in metapopulations along gradients of network configuration, dispersal categories (low 0.001 ; high >0.001), spatial-temporal (ST) correlations (low $\rho=0$; high $\rho=0.6$), scale of lognormal variance in recruitment (low $\sigma=0.001$; high $\sigma=0.1$), and spatial distribution of disturbance.

218 Next, we show violin plots demonstrating some of the modulating factors leading to variation in long-term impacts
 219 to patch occupancy.

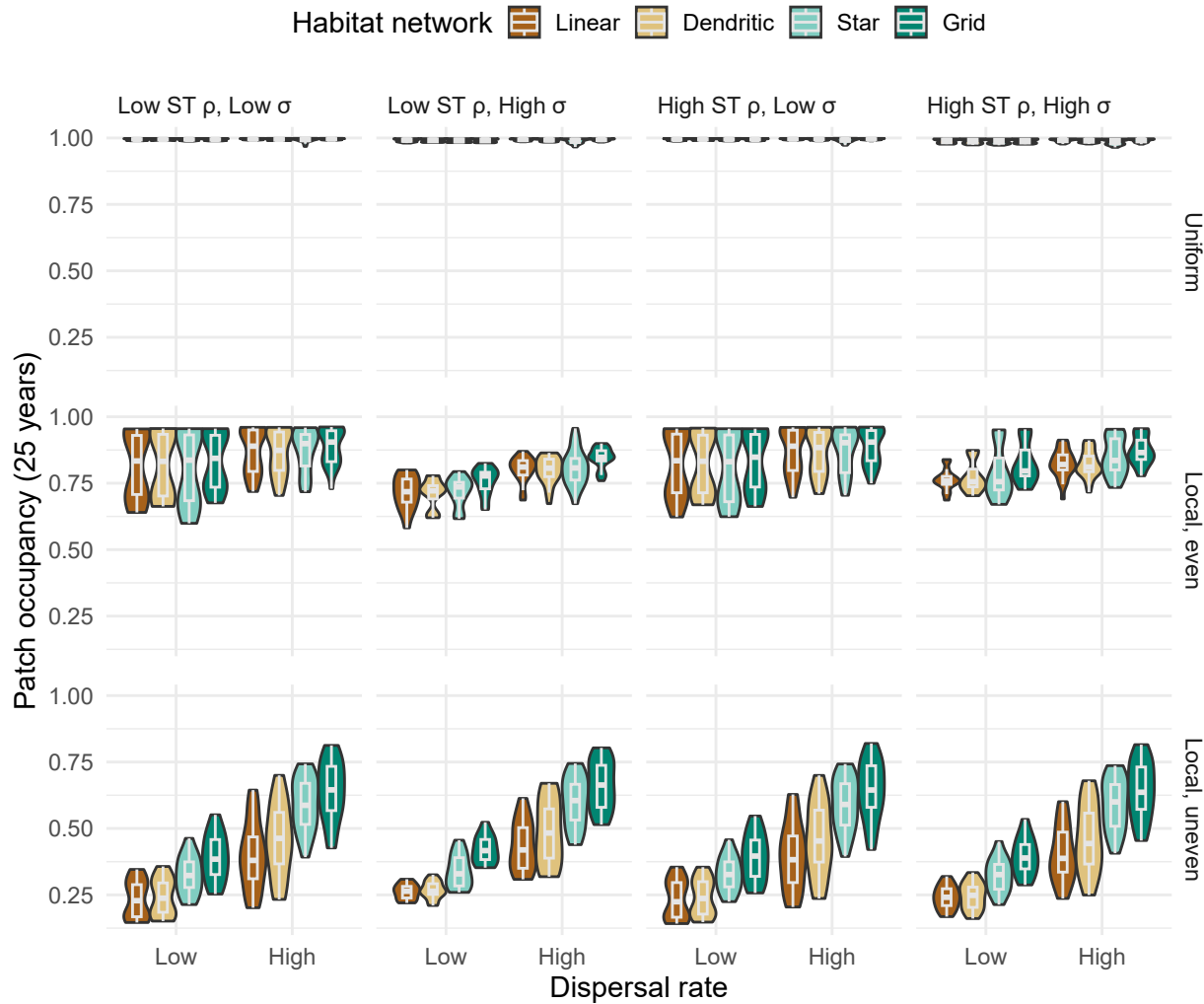


Figure S17: Violin plots showing marginal response of long-term patch occupancy in metapopulations along gradients of network configuration, dispersal categories (low 0.001; high > 0.001), spatial-temporal (ST) correlations (low ρ 0; high $\rho=0.6$), scale of lognormal variance in recruitment (low $\sigma= 0.001$; high $\sigma=0.1$), and spatial distribution of disturbance.

²²⁰ Next, we show variation in relative production metrics. Figure S13 shows the tight correlation between patch
²²¹ occupancy and relative production. Hence, Figure S17 and S18 look quite similar.

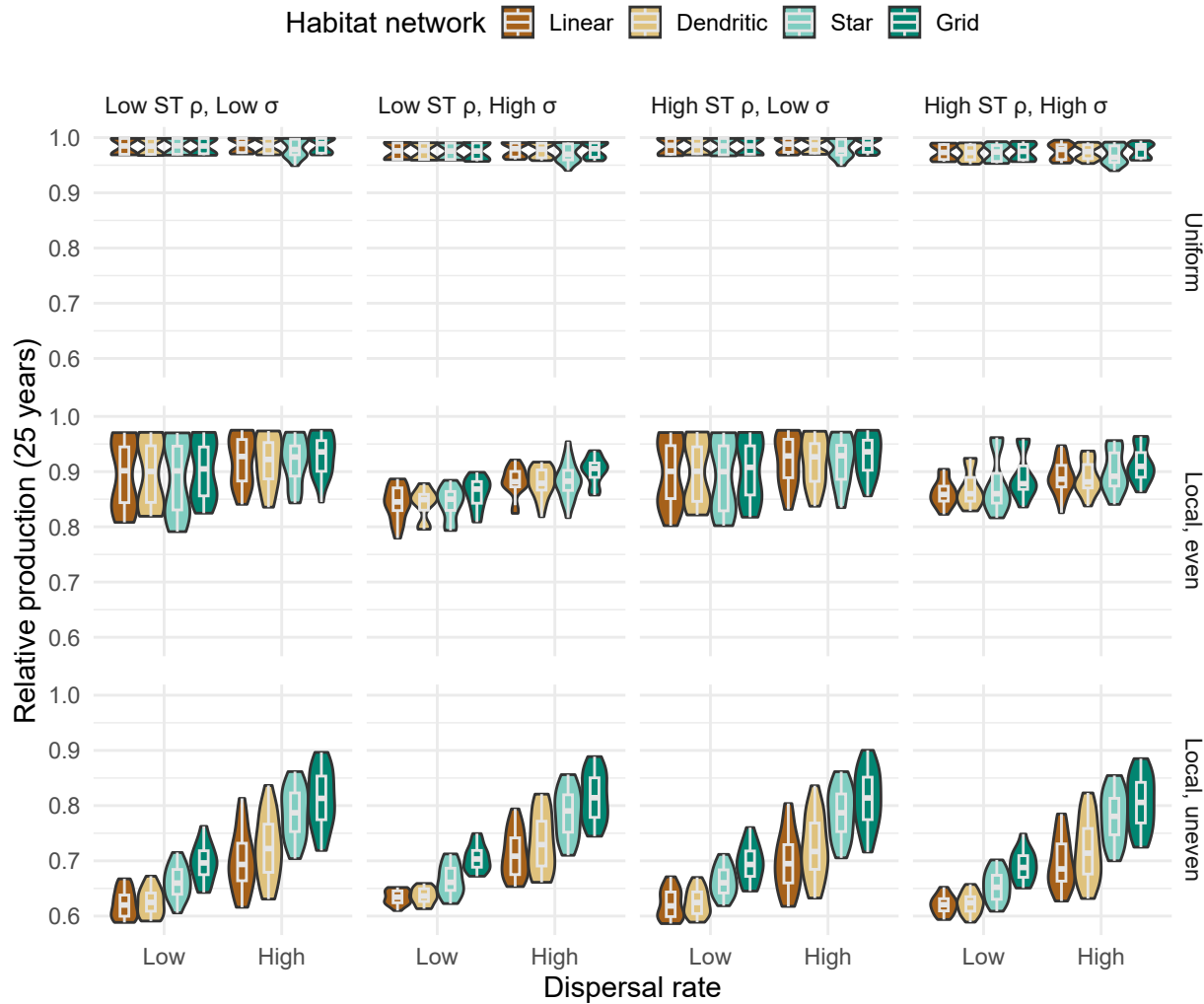


Figure S18: Violin plots showing marginal response of relative production for metapopulations along gradients of network configuration, dispersal categories (low 0.001; high >0.001), spatial-temporal (ST) correlations (low $\rho=0$; high $\rho=0.6$), scale of lognormal variance in recruitment (low $\sigma=0.001$; high $\sigma=0.1$), and spatial distribution of disturbance.

222 Dispersal, network topology, variable local demography, spatial-temporal correlations, and recruitment stochasticity
 223 also affected metapopulation recovery patterns in three key ways, though to a lesser extent. First, recovery rates
 224 increased with increased dispersal. However, this effect was nonlinear with diminishing benefits of dispersal
 225 occurring at ~1-3%, depending on spatial structure and disturbance. Second, more linearized networks had slower
 226 recovery times than more connected networks suggesting that rescue effects take some time to cascade through the
 227 entire network of patches; but this interacted with the disturbance regime as only local, extirpation exhibited this
 228 change in any substantial manner. Last, diversity in local patch compensation and carrying capacities tended to
 229 slow metapopulation recoveries - this effect interacted with other factors like stochasticity.

230 Section S1.6: Clustering analyses

231 We used hierarchical clustering analyses (implementing Ward's criterion) of a dissimilarity matrix from our four
232 recovery metrics to evaluate whether there was evidence for common recovery regimes among our simulation results
233 across all ecological and disturbance scenarios (Murtagh & Legendre 2014). Based on advice laid out in Hennig
234 (2014), we determined that the best number of unique clusters in metapopulation recoveries should satisfy the
235 following statistical criteria:

- 236** 1. recovery outcomes from within a cluster are closer to one another than to other clusters (i.e., the two Dunn
237 indices are relatively high)
- 238** 2. the number of clusters explains much of the point variation within the dataset (i.e., diminishing returns in
239 minimizing the sums-of-squared residuals)
- 240** 3. the point observations within clusters are relatively tight (i.e., both the average silhouette width and the
241 widest within-cluster gap are relatively low)
- 242** 4. clusters are relatively unique and there is good separation between the clusters (i.e., the separation index is
243 still high, while considering that low numbers of clusters should always have the highest separation)

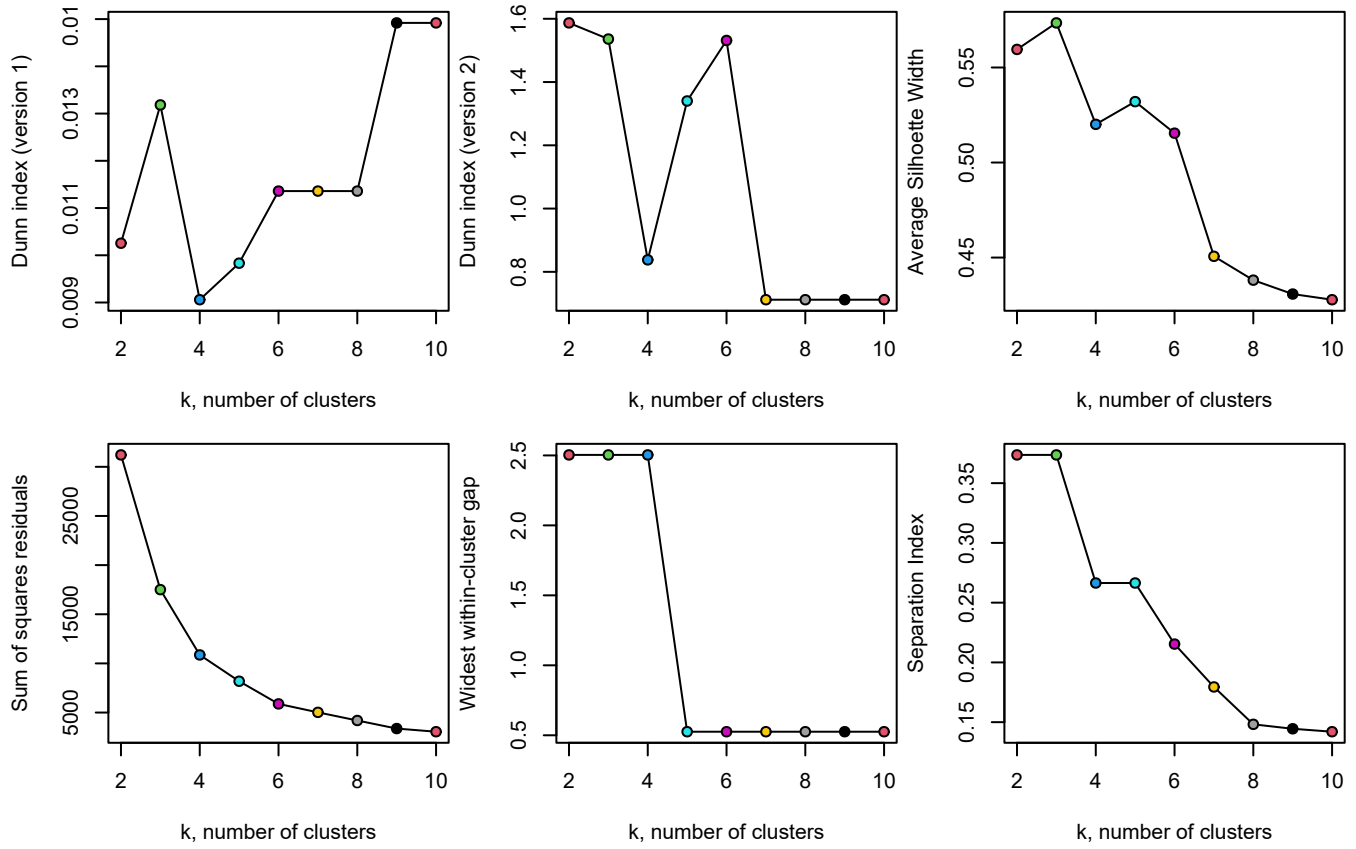


Figure S19: The relationships between number of potential clusters and multiple statistical criteria used to test support for the best number of clusters within the simulated recovery outcomes.

244 Based on the above criteria, we chose 5 unique clusters as satisfying most of the above criteria in the figure above,
245 although there was good support for between 3 and 6 unique clusters. The principal components analysis indicates
246 that five clusters has substantial explanatory power of metapopulation recovery metrics (explained ~89% of the
247 point variation).

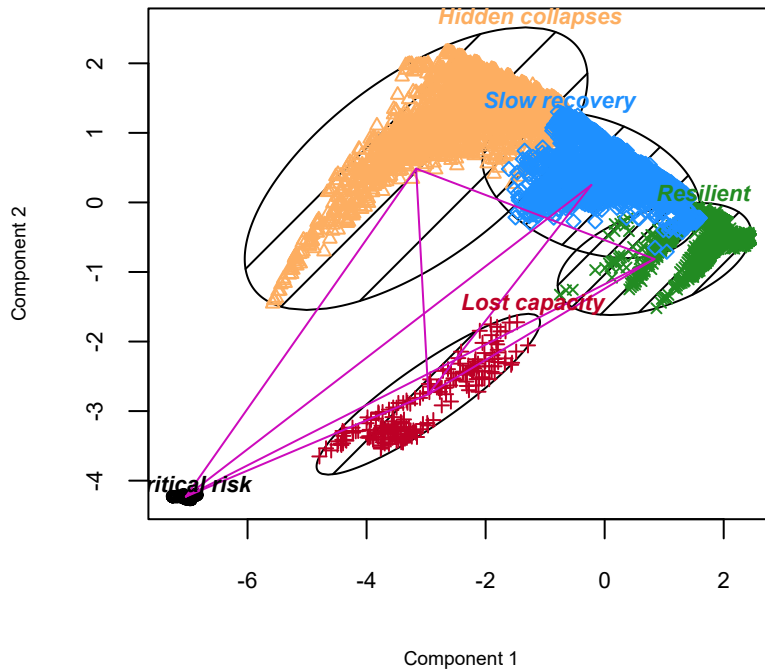


Figure S20: Bivariate cluster plot of the principal components explaining point variation in metapopulation recovery metrics across all simulated scenarios grouped into five distinct clusters.

248 **Section S1.6.1: Emergent recovery outcomes**

249 Overall, we used hierarchical clustering analyses to describe five common metapopulation recovery outcomes. These
 250 outcomes were: (1) resilient recovery – metapopulations recovered to pre-disturbance abundances quickly with all
 251 patches occupied, (2) slow recovery – were either slowed (compared to resilient recoveries), had reduced patch
 252 occupancy, or reduced relative production, (3) hidden collapses – metapopulations tended to recover and aggregate
 253 abundances were high, but many local patches remained unoccupied and recovery was slowed, (4) lost capacity –
 254 recovery rates were very slow, the risk of non-recovery was high, long-term production was low, and many local
 255 patches remained unoccupied and (5) critical risk – where metapopulations failed to recover, abundances remained
 256 low, and the risk of non-recovery was high.

Table S2: The mean recovery metrics, total sample size per regime (No.), and metapopulation abundance (N/K) for each of five common metapopulation recovery regimes supported by hierarchical clustering analyses across gradients in disturbance and network structure.

Regime	Network	Disturbance	No.	Recovery rate	% non-recovery	Occupancy	Relative production	Relative abundance
Resilient	Linear	Uniform	792	0.83	2	0.99	0.98	1.00
Resilient	Dendritic	Uniform	792	0.82	2	0.99	0.98	0.99
Resilient	Star	Uniform	792	0.81	3	0.99	0.98	0.99
Resilient	Grid	Uniform	792	0.82	2	0.99	0.98	1.00
Resilient	Linear	Local, even	205	0.78	5	0.94	0.95	0.99
Resilient	Dendritic	Local, even	201	0.78	5	0.94	0.96	0.99
Resilient	Star	Local, even	274	0.75	7	0.93	0.95	0.99
Resilient	Grid	Local, even	215	0.78	5	0.94	0.96	0.99
Slow recovery	Linear	Local, even	528	0.69	3	0.77	0.87	0.99
Slow recovery	Dendritic	Local, even	533	0.70	3	0.77	0.87	0.99
Slow recovery	Star	Local, even	466	0.68	5	0.75	0.86	0.99
Slow recovery	Grid	Local, even	529	0.73	3	0.81	0.89	0.99

Slow recovery	Linear	Local, uneven	11	0.72	0	0.64	0.81	1.00
Slow recovery	Dendritic	Local, uneven	69	0.73	0	0.66	0.81	0.99
Slow recovery	Star	Local, uneven	114	0.74	4	0.71	0.84	0.97
Slow recovery	Grid	Local, uneven	244	0.76	0	0.73	0.85	1.00
Hidden collapses	Linear	Local, even	9	0.61	3	0.59	0.79	0.99
Hidden collapses	Dendritic	Local, even	9	0.65	0	0.59	0.78	0.99
Hidden collapses	Star	Local, even	4	0.72	0	0.55	0.76	1.00
Hidden collapses	Linear	Local, uneven	709	0.34	21	0.34	0.67	0.97
Hidden collapses	Dendritic	Local, uneven	651	0.49	8	0.36	0.68	0.99
Hidden collapses	Star	Local, uneven	606	0.57	9	0.45	0.72	0.99
Hidden collapses	Grid	Local, uneven	476	0.56	7	0.46	0.73	0.99
Lost capacity	Linear	Local, even	50	0.17	77	0.58	0.79	0.66
Lost capacity	Dendritic	Local, even	49	0.16	78	0.58	0.78	0.65
Lost capacity	Star	Local, even	48	0.16	78	0.58	0.78	0.65
Lost capacity	Grid	Local, even	48	0.16	79	0.57	0.78	0.64
Critical risk	Linear	Local, uneven	72	0.00	100	0.10	0.54	0.09
Critical risk	Dendritic	Local, uneven	72	0.00	100	0.10	0.54	0.08
Critical risk	Star	Local, uneven	72	0.00	100	0.10	0.54	0.08
Critical risk	Grid	Local, uneven	72	0.00	100	0.10	0.54	0.08

257 In general, the five recovery regimes spanned a continuum of better (e.g., resilient) to worse recoveries (e.g.,
 258 long-term critical risks). Overall, the interplay between ecological and disturbance conditions appeared to structure
 259 the specific pathway for metapopulation recoveries (Figure S21; Table S2). For example, uniform disturbances
 260 always led to resilient recoveries. However, local, even disturbance regimes tended to lead to, at-best, a resilient
 261 recovery or, at worst, hidden collapses with the probability modulated by other ecological factors. Local, uneven
 262 disturbance regimes led to, at best, a slow recovery or, at worst, a long-term critical risk and non-recovery. The
 263 main text Figure 5 and 6 demonstrates the conditions that led to resilient recoveries compared to critical risks,
 264 while more intermediate outcomes, like slow recovery, hidden collapses, or lost capacity are shown here in Figures
 265 S22-S24.

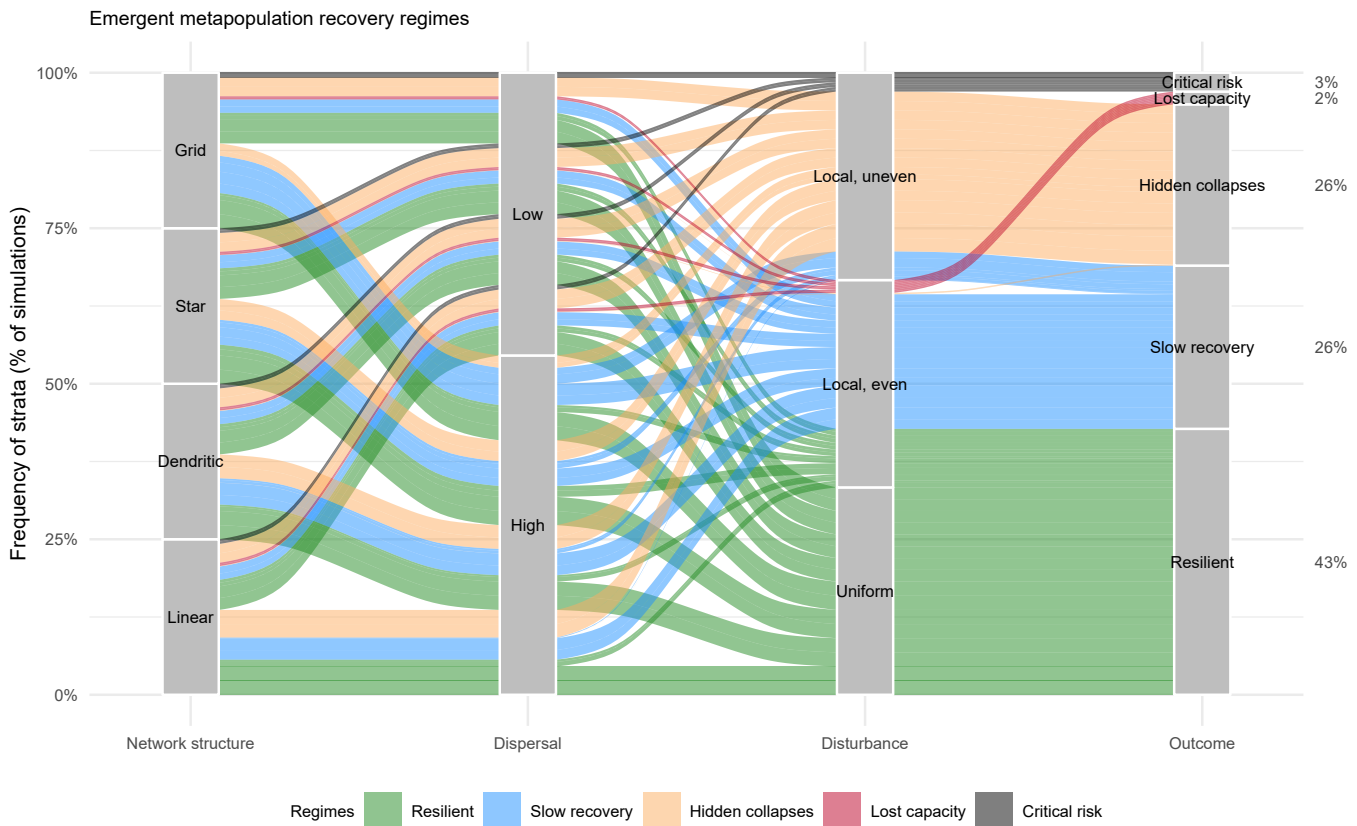


Figure S21: Frequency of emergent metapopulation recovery regimes can depend on a complex interplay between network structure, dispersal, and spatial disturbances. Ribbon colors denote a group of simulations that led to one of five common recovery outcomes. Frequency of regimes denoted by width of ribbons

266 Section S1.6.2: Role of ecological and disturbance conditions on recovery outcomes

267 Local patch demography, habitat network structure, dispersal, spatially and temporally correlated recruitment
 268 variation, and spatial disturbance regimes each had modulating effects on the probability for any particular
 269 recovery regime (Figures 5 & 6 in the main text; and Figures S22-S24 here). There was a clear signal from any
 270 localized disturbances, which increased the probability for non-resilient recovery regimes. For habitat networks,
 271 metapopulations with linear networks tended to have increased probability for worse recoveries compared to
 272 gridded networks. For dispersal rates, metapopulations with low dispersal had increased probability for poor
 273 recoveries compared to high dispersal. For local demography, metapopulations with variable local patch
 274 demographic rates tended to increased probability for poor recoveries compared to metapopulations composed of
 275 homogeneous local patches. For recruitment stochasticity, metapopulations with both high recruitment variation
 276 and high spatial-temporal correlations led to increased probability for poor recoveries compared to low variation
 277 and low correlations.

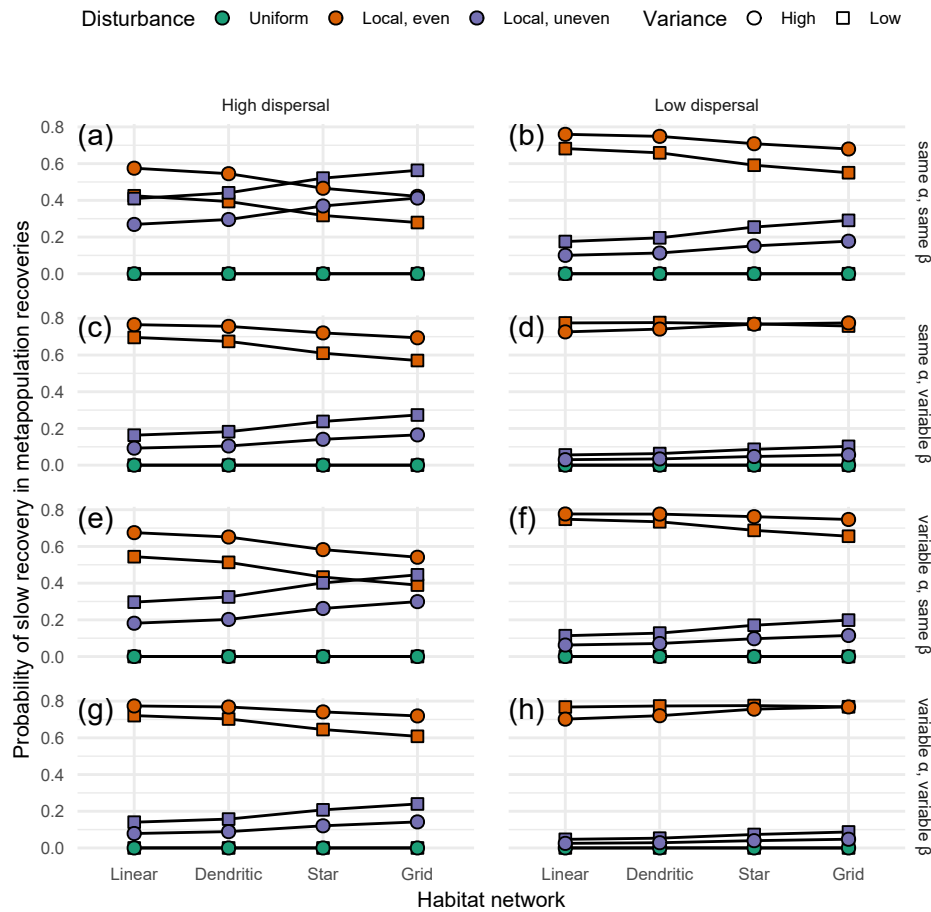


Figure S22: The probability of a slow recovery in metapopulation recoveries depended on the interplay between network structure, dispersal (low 0.001; high>0.001), spatial disturbances, heterogeneity in local demographic rates (α is local patch productivity and β is local patch carrying capacity), and spatial-temporal recruitment variation (high= $\rho=0.6$ and $\sigma=0.1$; low= $\rho=0$ and $\sigma=0.001$) based on ordered logistic regression.

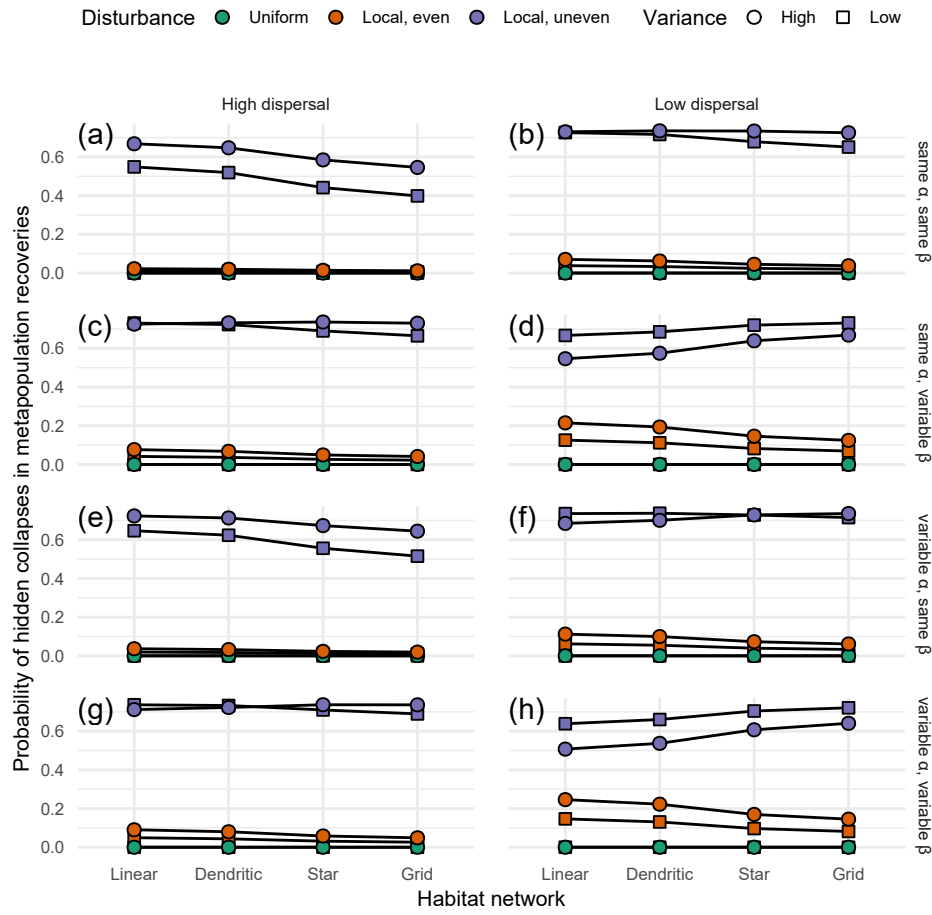


Figure S23: The probability of hidden local collapses in metapopulation recoveries depended on the interplay between network structure, dispersal (low 0.001; high > 0.001), spatial disturbances, heterogeneity in local demographic rates (α is local patch productivity and β is local patch carrying capacity), and spatial-temporal recruitment variation (high = $\rho=0.6$ and $\sigma=0.1$; low = $\rho=0$ and $\sigma=0.001$) based on ordered logistic regression.

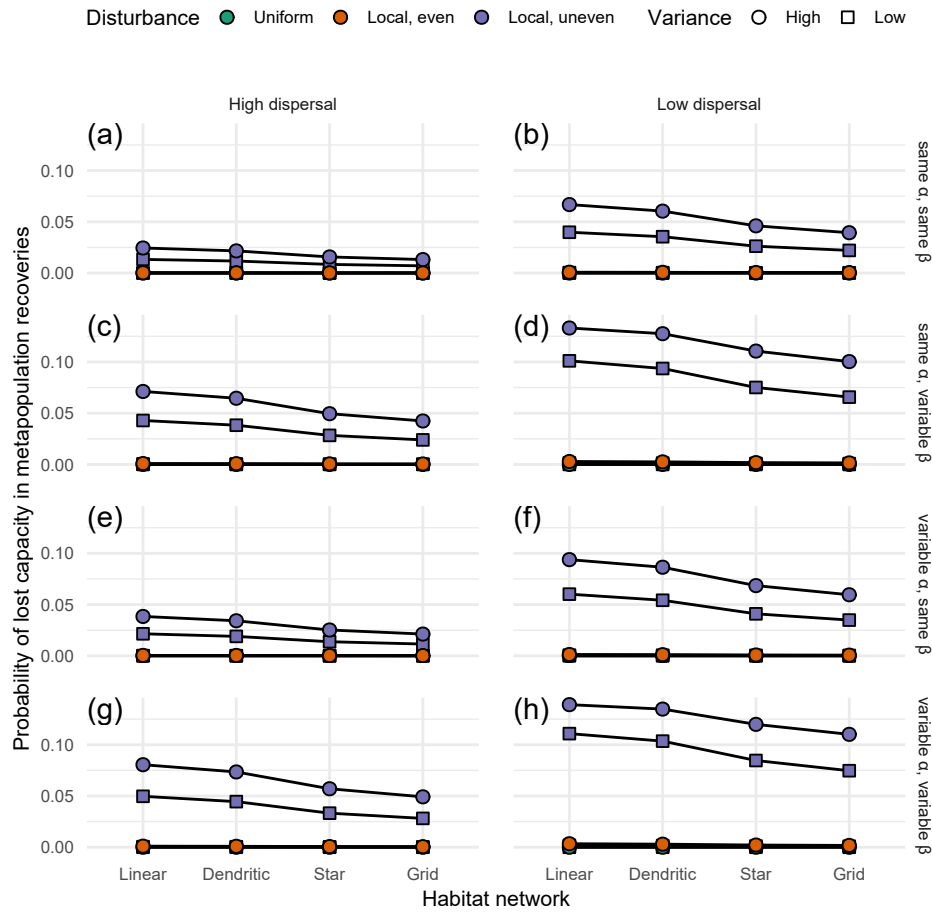


Figure S24: The probability of lost productive capacity in metapopulation recoveries depended on the interplay between network structure, dispersal (low 0.001; high > 0.001), spatial disturbances, heterogeneity in local demographic rates (α is local patch productivity and β is local patch carrying capacity), and spatial-temporal recruitment variation (high = $\rho=0.6$ and $\sigma=0.1$; low = $\rho=0$ and $\sigma=0.001$) based on ordered logistic regression.

278 Section S1.7: References

- 279 Anderson, S.C., Moore, J.W., McClure, M.M., Dulvy, N.K. & Cooper, A.B. (2015). Portfolio conservation of
280 metapopulations under climate change. *Ecological Applications*, 25, 559–572.
281 Bowlby, H.D. & Gibson, A.J.F. (2020). Evaluating whether metapopulation structure benefits endangered
282 diadromous fishes. *Canadian Journal of Fisheries and Aquatic Sciences*, 77, 388–400.
283 Csardi, G. & Nepusz, T. (2006). The igraph software package for complex network research. *InterJournal*,
284 Complex Sy, 1695.
285 Forrest, R.E., McAllister, M.K., Dorn, M.W., Martell, S.J.D. & Stanley, R.D. (2010). Hierarchical Bayesian
286 estimation of recruitment parameters and reference points for Pacific rockfishes (*Sebastodes* spp.) under
287 alternative assumptions about the stock-recruit function. *Canadian Journal of Fisheries and Aquatic Sciences*,
288 67, 1611–1634.
289 Fullerton, A.H., Anzalone, S., Moran, P., Van Doornik, D.M., Copeland, T. & Zabel, R.W. (2016). Setting spatial
290 conservation priorities despite incomplete data for characterizing metapopulations. *Ecological Applications*, 26,
291 2558–2578.
292 Hennig, C. (2014). How many bee species? A case study in determining the number of clusters. In: *Data analysis,*
293 *machine learning and knowledge discovery* (eds. Spiliopoulou, M., Schmidt-Thieme, L. & Janning, R.). pp.
294 41–49.
295 Moore, J.W., Connors, B.M. & Hodgson, E.E. (2021). Conservation risks and portfolio effects in mixed-stock
296 fisheries. *Fish and Fisheries*, faf.12567.
297 Murtagh, F. & Legendre, P. (2014). Ward's hierarchical agglomerative clustering method: which algorithms
298 implement Ward's criterion? *Journal of Classification*, 31, 274–295.
299 Myers, R.A., Bowen, K.G. & Barrowman, N.J. (1999). Maximum reproductive rate of fish at low population sizes.
300 *Canadian Journal of Fisheries and Aquatic Sciences*, 56, 2404–2419.
301 Okamoto, D.K., Hessing-Lewis, M., Samhouri, J.F., Shelton, A.O., Stier, A.C., Levin, P.S. & Salomon, A.K. (2020).
302 Spatial variation in exploited metapopulations obscures risk of collapse. *Ecological Applications*, 30, e02051.

- 303 Walters, C.J. & Martell, S.J.D. (2004). *Fisheries ecology and management*. Princeton University Press.
- 304 Yeakel, J.D., Moore, J.W., Guimarães, P.R. & Aguiar, M.A.M. de. (2014). Synchronisation and stability in river
305 metapopulation networks. *Ecology Letters*, 17, 273–283.
- 306 Zelnik, Y.R., Arnoldi, J. & Loreau, M. (2019). The three regimes of spatial recovery. *Ecology*, 100, e02586.